COLLECTIVE DYNAMICS OF KINESIN-1

by

Adam G. Hendricks

A dissertation submitted in partial fulfillment
of the requirements for the degree of
Doctor of Philosophy
(Mechanical Engineering)
in The University of Michigan
2008

Doctoral Committee:

Professor Edgar Meyhöfer, Co-Chair
Associate Professor Bogdan I. Epureanu, Co-Chair
Professor Karl Grosh
Associate Professor Alan J. Hunt

ACKNOWLEDGEMENTS

First, I would like to thank my advisors, Dr. Bogdan Epureanu and Dr. Edgar Meyhöfer, for allowing me the freedom to pursue a subject that was new to me, and for teaching me a great deal in the process. I would also like to thank the members of the Nanomechanics lab (Ming-Tse Kao, Neha Kaul, Troy Lionberger, and Diane Wiener) and the Epureanu lab (Kiran D'Souza and Arjun Krishnan) for their patience, time, and collaboration. Finally, I would like to thank my parents, for instilling in me a curiosity of how things work and my lovely wife for her constant support during this process. This material is based upon work supported under a National Science Foundation Graduate Research Fellowship.

TABLE OF CONTENTS

LIST OF FIGURES

Figure

ABSTRACT

Motor proteins are the engines of biology, converting chemical energy to mechanical work in cells. Kinesin-1 is a motor protein that transports vesicles towards the plus end of microtubules, widely believed to be responsible for anterograde transport of synaptic vesicles in neurons. Advances in single-molecule techniques have allowed the characterization of single kinesin motors in vitro at a range of loads and ATP concentrations. Single kinesin motors are capable of processive movement along the microtubule at a maximum velocity of approximately 1 μm/s. The velocity decreases roughly linearly in response to load until reaching stall at a load of approximately 6 pN. Several theoretical models have been proposed that describe the steady-state motion of single kinesin motors. However, growing evidence suggests that kinesin functions collectively in cells, whereby several motors work in a coordinated manner to transport a vesicle. A transient description is required to describe collective dynamics, as the interactions among coupled motors induce time-varying forces on each motor. Herein a mechanistic model of kinesin is proposed that is capable of accurately describing transient and steady-state dynamics. Each domain of the protein is modeled via a mechanical potential. The mechanical potentials are related explicitly to the chemical kinetics of each motor domain. The mechanistic model was used to simulate the collective behavior of coupled kinesin motors under varying loads, cargo linker stiffnesses, and numbers of motors. To analyze the simulations of coordinated transport, several metrics were developed that are specifically tai-

lored to characterizing the synchronization of nonlinear, nonsmooth oscillators like kinesin. The model results suggest that, in the cell, coupled motors under low loads are loosely correlated. When the load is increased, such as when the cargo encounters an obstacle like another vesicle or the cytoskeleton, motors become more correlated in response to increased loads, allowing them to produce greater forces. Increasing the number of motors involved in the transport does not appreciably increase the dimensionality of the trajectory, implying large numbers of motors are able to work collectively, even without becoming fully synchronized.

CHAPTER I

Introduction

Motor proteins convert chemical energy into mechanical work to perform diverse, vital roles in cells including vesicle transport, cell division, muscle contraction, cell motility, DNA and RNA replication, transcription, and remodeling of macromolecular assemblies (39, 46, 99, 101). They perform a multitude of vital roles and are present in all forms of life, from bacteria to humans. For instance, the motor protein myosin-1 is the active element in muscle contraction. Bacterial flagella are powered by motor proteins. Another class of motor proteins, dynein, power flagella and cillia in eukaryotes. The motor protein prestin is thought to provide the feedback mechanism that increases frequency differentiation and sensitivity in hearing. During mitosis, kinesin motors are implicated in the positioning of chromosomes during metaphase. Another kinesin motor then cleaves the two halves apart in anaphase. The ubiquity of motor proteins in biology means the understanding of their mechanochemical mechanisms has the potential for far-reaching impact in the fields of cell biology, medicine, and engineering.

One class of motor proteins, kinesins, use the energy from ATP hydrolysis to produce directed movement along microtubules. This dissertation focuses on kinesin-1, previously referred to as conventional kinesin or kinesin heavy chain (KHC) (69),

which is widely believed to be responsible for anterograde transport of synaptic vesicles in neurons (13, 101). Kinesin-1 is a heterotetramer that consists of two identical heavy chains (120 kDa) and two identical light chains (60 kDa), as seen in Fig. 1.1. At their *N*-terminal ends, the two heavy chains form globular head domains that hydrolyze ATP and bind to the microtubule. Alpha-helical segments in the neck and stock domains dimerize via coiled-coil formations C-terminally to the head domains. The C-terminal tail domains of the kinesin heavy chains bind the two light chains, which in turn interact with a variety of linker molecules to mediate the binding of cargoes (12, 22, 42, 62, 68, 87, 88, 104). We will refer to kinesin-1 simply as kinesin.

Advances in single-molecule *in vitro* motility assays of kinesin (10, 47), sophisticated laser trapping techniques (97, 98), and single molecule imaging experiments (106) have allowed initial characterizations of kinesin movement along microtubules and force generation. There is now general agreement that single kinesin motor proteins step processively along microtubules by tracking parallel to a single protofilament and advancing in discrete 8 nm steps, each of which is coupled directly to the hydrolysis of a single ATP molecule (1, 26, 33, 40, 43, 49, 80, 85). The observed stepping behavior is the result of alternately advancing kinesin heads, where the head in the rear position detaches, moves toward the plus-end of the microtubule and subsequently binds to a beta-tubulin binding site 16 nm ahead of its previous site, leading to an 8 nm advance of the centroid of the molecule.

The crystal structure of the monomeric kinesin KIF1A was solved by several researchers (64, 65, 77, 83), as shown in Fig. 1.2. The motor domain is expected to be conserved between KIF1A and kinesin-1. The binding of ATP results in a conformational change in the motor domain which is thought to induce mechanical

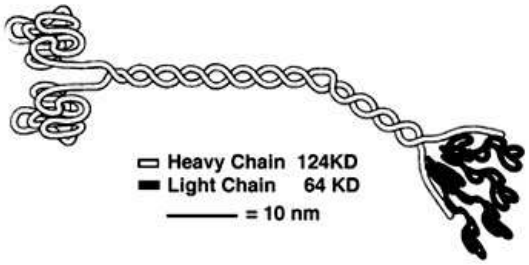

Figure 1.1: Sketch of kinesin-1. Taken from Hackney (41).

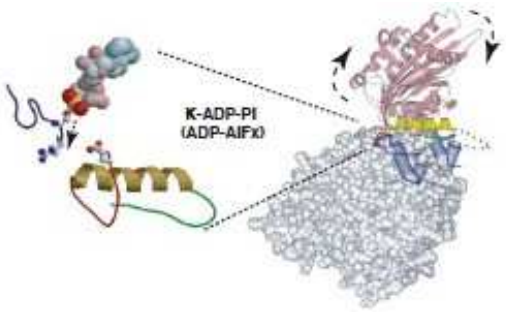

Figure 1.2: Crystal structure of the motor domain of KIF1A. Taken from Nitta et al. (77).

stresses in the molecule, and propel the rearward head forward.

Several researchers have characterized the effect of external loads on the movement of kinesin *in vitro*. In these experiments, the tail and/or stock domains of the kinesin molecule were adsorbed or chemically bound to micrometer-sized silica or latex beads and manipulated such that the head domains could interact with an immobilized microtubule in the presence of ATP. External forces were applied to the bead through an optical trap or flexible glass fibers (11, 17, 60, 73, 97, 102, 105), and the effect on the velocity of the motor was observed (see Figs. 1.3 and 1.4). These measurements resulted in force-velocity curves for a range of ATP concentrations. Taken together, they show that the maximum force against which a single kinesin motor can advance is about 6 pN and the relationship between force and velocity is approximately linear at moderate loads ($2 - 4$ pN).

While considerable attention has been paid to the mechanics of single kinesin motors, much less attention has been given to the collective behavior of kinesin, despite evidence that in the cell each cargo is transported by several kinesin motors working in concert (37, 39, 100). The goal of this study is to provide a link between the wealth of single-molecule data on kinesin and the behavior of kinesin in intra-

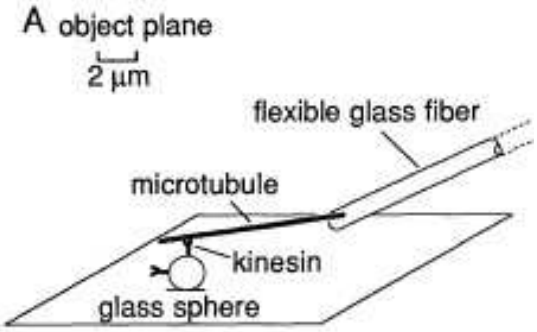

Figure 1.3: Forces were applied to the motor through flexible glass fibers. Taken from Meyhöfer and Howard (73).

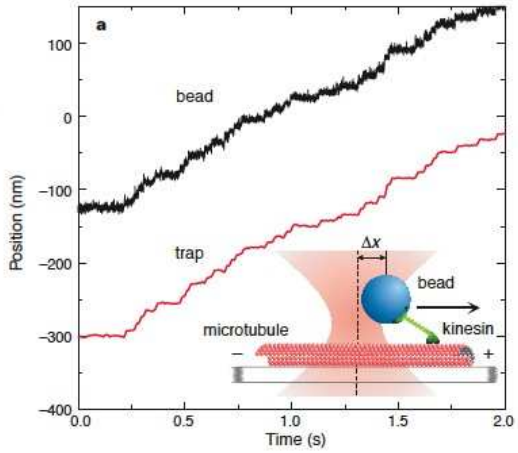

Figure 1.4: Forces were applied to the motor through an optical trap. Taken from Visscher et al. (105).

cellular transport, where it is likely that kinesin motor proteins work collectively. Specifically, the study aims to answer questions such as: do coupled kinesin motors synchronize, or function largely independently? Howard et al. (47) made an early observation that the speed of transport in a gliding assay is *independent* of the number of motors interacting with the microtubule. How do large numbers of motors interact such that the speed is unaffected? What advantage does kinesin gain by working in teams? There is a cost associated with expending more ATP, so there must also be a significant benefit, such as increased processivity or the ability to exert larger forces. The study also aims to develop the tools necessary to characterize the dynamics of nonlinear, nonsmooth coupled oscillators such as kinesin. Much of the previous work on coupled oscillators focused on simple, one degree-of-freedom oscillators (19, 67, 92, 94). Oscillators such as kinesin exhibit multiple time scales in the cycle, are nonlinear due to the effect of force on diffusion, and are nonsmooth as the equations of motion are unique for each chemical state.

A model-driven approach is used in this study. A mathematical model forces

one to make explicit assumptions where there are unknowns, and the effect of these assumptions on the results of the model can be quantified. A mathematical model also allows one to test the effect of a large number of variables, and identify those best suited for experimental inquiry. In this way, the model can be used to design experiments and the results of the experiment can be compared quantitatively to the predictions of the model. A model-driven approach is implemented in this study by first developing a mathematical model based on current data from single-molecule experiments and structural data. The model is then used to make quantitative predictions of the collective dynamics of kinesin.

An in-depth understanding of kinesin behavior in the cell is vital to cell biology, medicine, and engineering nano-scale devices. For example, the degradation of intracellular transport performed by kinesin-1 is implicated in neurodegenerative diseases such as Alzheimer's and Parkinson's disease (34, 89). In addition, an understanding of kinesin-1 may have applications to cancer therapies, as two major drugs used to treat cancer, Taxol and Monastrol (56, 72, 84), function by disrupting closely-related kinesins involved in cell replication. Ultimately, the transport machinery of cells, i.e. motor proteins, could be used to perform targeted drug delivery. Biological motors can also be used to power nanoscale devices, such as for molecular sorting and lab-on-a-chip applications (45, 71, 103).

1.1 Background and Motivation

On the basis of single molecule mechanical measurements, structural data (64, 65, 83), and detailed insights into the biochemical transduction cycle of kinesin (20, 32, 81), several models have been proposed to quantitatively explain the mechanism by which chemical energy from ATP hydrolysis is converted to directed move-

ment by kinesin motors. Existing quantitative models of motor proteins can be classified as kinetic models or thermal ratchet models. Kinetic models describe the mechanochemical cycle as a set of discrete states with stochastic, reversible transitions between them (28–30, 57). The model of Peskin and Oster (78), although derived from mechanical arguments, can also be considered a kinetic multi-state model as the bead is considered to diffuse infinitely fast, reducing the model to a Markov chain. Each state represents a point in the ATP hydrolysis cycle, so that one 8 nm step is coupled to the hydrolysis cycle of one molecule of ATP. Kinetic models have been successful in providing simple, closed-form relationships that describe the steady-state motion of kinesin by relating the measured force-velocity data to kinetic parameters. This approach has also been extended to describe dissociation from the microtubule (61). Existing kinetic models are able to describe the steady-state behavior of single kinesin motors, such as the motion under a constant load. Although kinetic models have been used to describe coupled motor proteins (95, 96), the description is inadequate as kinetic models are only able to model transients due to the initial probability distribution, and cannot properly handle time-varying loads because a quasi-steady approximation is made. This approximation is adequate only when the transition rates are dependent on a constant or slowly-varying load, so that the transient dynamics at fast timescales can be considered negligible. Furthermore, the dynamics are only defined at a small number of discrete spatial locations (2-4 per step in current models). Thus in these models the coupling between motors, which is dependent on all motor locations, cannot be accurately resolved.

Thermal ratchet models view the motor as a single particle, or a group of particles, in stochastically-switched potentials (2, 3, 9, 31, 53, 54, 59, 107). Thermal ratchet models have been successful in describing the steady-state force-velocity data and

statistical behavior for single molecules, and have also been used to explain the directionality of motors (3). An extension of the thermal ratchet model was made by Bier (6, 7) where part of the motion of the diffusing head is considered to be a deterministic power stroke. This approach showed that a deterministic power stroke coupled with a random search could result in an almost four-fold enhancement of diffusion. Using methods similar to thermal ratchet models, Derenyi and Vicsek (23) model kinesin as two elastically coupled Brownian particles. Thermal ratchet models have the advantage of a well-developed formalism, convenient calculations and simulations, and a small number of parameters. However, these models must define potentials *a priori*, before solving for the motion of the motor(s). Thus, they cannot account for potentials that are dependent on the instantaneous coupling between motor domains or among multiple motors.

In addition to the steady-state behavior, the focus herein is on the *transient* dynamics of kinesin movement, at both slow and fast timescales. For instance, how does the motor respond to a sudden change in load? What is the stability of the mechanochemical cycle, i.e. limit cycle (38, 92), to perturbations? Answers to these questions will lead to better understanding of the interaction between individual motor domains of a single motor molecule and among multiple motor molecules transporting a common load. Although there is little direct evidence (37, 39, 100), it is generally believed that inside cells, several kinesin motors work in concert to transport vesicles. Recently, Kural et al. (66) reported high resolution fluorescence observations of the movement of GFP-tagged peroxisomes in intact cells. Their observations suggest that multiple kinesins interact in a *coordinated manner* such that vesicle transport occurs at up to 10 times the *in vitro* gliding speeds of kinesin. Levi et al. (70) observed similar results using brightfield transmission light microscopy

of pigment-filled melanosomes. Using an analogous approach, Nan et al. (76) used endocytosed quantum dots to visualize microtubule-based transport in intact cells. They observed step sizes of 8 nm and 16 nm due to kinesin, and hypothesized that the 16 nm steps may be due to the coordination between multiple motors. By tracking individual quantum dot tagged motors, Courty et al. (18) found evidence that cooperation among motors leads to greater processivity. Cai et al. (14) tracked single fluorescently-labelled motors in mammalian cells and observed speeds and run lengths of single kinesin motors in vivo are analogous to in vitro measurements. Diehl et al. (24) observed that engineered assemblies of two and three motors increased the speed of gliding assays by a factor of two over single motors. Theoretical work by Badoual et al. (4) proposes that the directionality in a multiple motor gliding assay is a property of the *ensemble of motor molecules* and not entirely determined by the single-molecule characteristics of a motor molecule. Badoual's proposal also opens intriguing possibilities for the regulation of the directional control of intracellular vesicle transport, which involves both plus- and minus-end directed motors.

The dynamic model presented herein is designed to capture transient dynamics which must be accurately described to correctly characterize the interaction of individual head domains in a single kinesin motor molecule and the interactions among groups of motor proteins, as the coupling results in unsteady forces on each motor domain. Previous approaches, where a quasi-steady approximation is made, are adequate for describing slow timescales, on the order of the stepping period. However, coupling between motors may result in dynamics at much faster timescales. Methods exist that are capable of describing stochasticity and transients, such as Monte Carlo simulations. However, they are computationally extremely expensive. A mechanistic approach allows efficient characterization of the transient dynamics at

slow and fast timescales. Such a mechanistic model is constructed in this paper by starting from simplified models of the main components of kinesin, and their known primary functions. In particular, the model includes simplified representations of the mechanical energy storage in all domains, and the resulting characterization of how forces (stresses) are distributed throughout all domains of the motor. Next, each domain is modeled from a mechanistic perspective by characterizing the relation between load and chemical kinetics. This characterization is done for the fully unsteady response of each domain (i.e. the response caused by time and space varying external loads and stresses between domains or motors). The mechanistic models for each domain are then combined to obtain the full model for one motor and for a number of coupled motors. Such an approach ensures that *all* mechanistic couplings between domains are taken into account. Consequently the model presented herein is capable of predicting both steady-state and transient dynamics. The overall effect of unsteady loads on kinesin dynamics is related explicitly to the molecule structure and chemical kinetics, thus providing insight into the mechanochemical cycle.

CHAPTER II

Description of the Model

The mechanistic model is based on the following structure: two identical heads are connected via identical domains (neck linkers) to a neck, as shown in Fig. 2.1. An additional domain (cargo linker) composed of the tail domain and the linker molecules connects the neck to the bead. Each head has three structural states, with each state defining the affinity to the microtubule binding site and the equilibrium position of the neck with respect to the heads.

The model is based on four key aspects: the mechanical properties of each domain, the chemical kinetics and its dependence on stresses in the molecule, the Brownian motion under time and space dependent loads (caused by couplings with other motor domains or by external factors), and the affinity of the heads to the microtubule binding sites. These aspects are coupled to form a complete model. In the following, each key aspect is discussed.

First, the mechanical characteristics of each domain are modeled. To obtain a simple mathematical representation, the mechanical energy stored in each domain is modeled via a mechanical potential. This potential corresponds to considering each domain as an elastic element with simple mechanical properties. Quadratic potentials are used for characterizing these elements, which can then be thought of

as simple, linear elastic elements (for each domain). The quadratic forms chosen for these potentials are the simplest possible forms (for non-constant forces), and correspond to first-order approximations of deformation-load relationships. More complex forms for the potentials of each domain could easily be incorporated into this approach.

Second, the dependence of the chemical kinetics on the *unsteady* stresses in the molecule are modeled. Directed movement is the combined result of conformational transformations, the relaxation of internal stresses, and Brownian motion. In the proposed model, the mechanochemical cycle proceeds as follows. Beginning with both heads at a binding site, the rear head is in the weakly-bound state (1) and the front head is in the strongly-bound state (3). The stresses in the elastic elements, and the resulting (unsteady) forces propel the rear head forward. Brownian motion pushes the head the remaining distance to the next binding site, working against the (time and space varying) internal stresses in the molecule. Once the diffusing head reaches the binding site, the head is assumed to be in state (2) and have a high affinity to the microtubule. The majority of the time is spent in this mechanochemical state, with both heads having high affinity to the microtubule, but in opposite structural states (rear head in state (3) and front head in state (2)). A single chemical state variable is used to describe the state of the two heads. While the weakly-bound head (state (1)) is diffusing, the chemical state variable is approximately constant. Once the head reaches the binding site (state (2)), the chemical state variable becomes active. The structural states of both heads switch when the chemical state variable reaches plus or minus 1, causing the front head to switch to the strongly-bound state (3) and the rear head to be in the weakly-bound state (1). For simplicity, we assume that both motor domains switch states simultaneously. Experiments have

shown that the dependence of the mechanochemical cycle on ATP concentration at constant loads can be described by Michaelis-Menten kinetics (for example see Visscher et al. (105)), characteristic of enzymatic reactions. Therefore, we assume that each individual head domain also follows Michaelis-Menten kinetics (27, 63, 74). The dependence of the chemical kinetics on the stresses in the molecule (i.e. its dynamic configuration) is assumed to be in a form such that an optimal strain for the chemical reaction exists. A strain/configuration away from the optimum results in a slower chemical reaction.

Third, the influence of Brownian motion under a space and time varying load is modeled using a novel approach inspired by the closed-form solution for the mean first-passage time (5). As the motor proceeds forward, the time and space varying forces on the diffusing head are recorded at each intermediate position. The forces on the head for the remaining distance to the binding site are then estimated. Using the resulting potential function, we calculate the mean first-passage time for the distance between binding sites. Given the time and distance to be traveled, we calculate the average velocity needed to reach the binding site at the mean first-passage time. The calculation is repeated at each instant of the motion. To demonstrate this algorithm, a particle diffusing under an arbitrary space and time varying load was simulated, as shown in Fig. 2.2. The particle is shown to reach the final position at the mean first-passage time of the actual, time-varying potential (calculated using the closed-form solution) with a high degree of accuracy, even for complicated potential functions. In Fig. 2.2, the projected force was estimated as constant over an infinitesimal interval starting at each instantaneous state. However, in the proposed kinesin model, a more complex and accurate estimate of the potential is used, based on the potentials of each domain, and the couplings between domains. The ability of the potential to

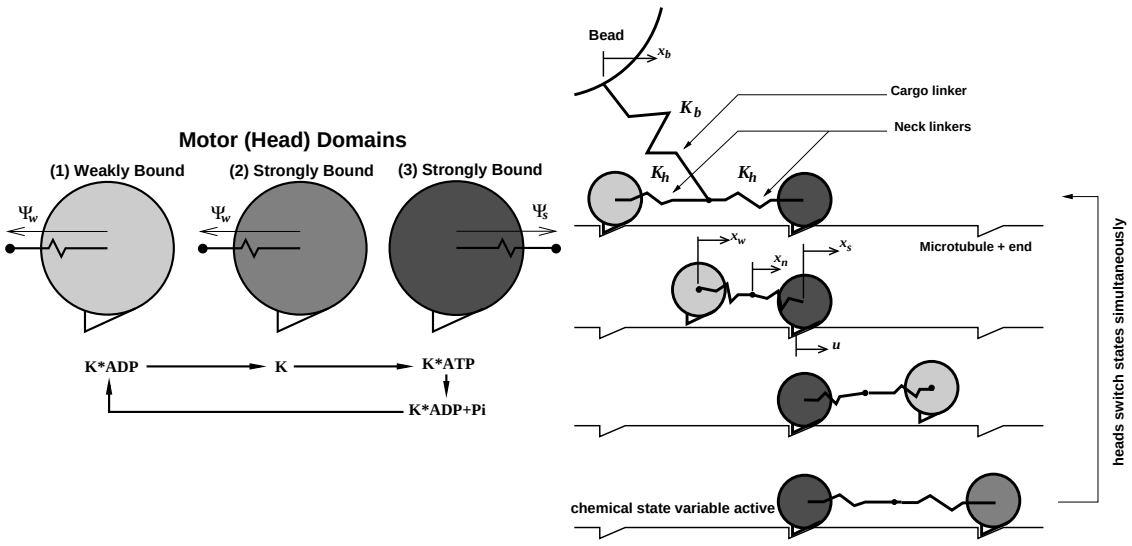

Figure 2.1: Left: Structural States - Each motor domain has three states corresponding to the nucleotide state. The structural state is described by the equilibrium position of the neck with respect to the head, Ψ, and the affinity to the microtubule binding site. Right: Mechanistic Model - Stresses, induced in the domains of the molecule through the conformational change, propel the rearward head forward. Brownian motion then pushes the head to the next unoccupied binding site, where the structural state of the heads switches simultaneously and the cycle is repeated.

vary in time is a key attribute that enables us to obtain a *transient, deterministic* model of the motor dynamics, which predicts accurately the average motion of the motor.

Fourth, the potential in which each head diffuses is influenced by the stresses in the elastic elements and also by the affinity of each head to the microtubule. The affinity of each head to the microtubule is modeled through potential wells centered at the binding site locations. Naturally, the head has a high affinity to the microtubule binding site if it is in the strongly-bound state. The weakly-bound state is assumed to have a much lower affinity (by a factor of approximately 10^3) to the binding sites. Also, the affinity of the binding sites is assumed to act on the heads only when the heads are near unoccupied binding sites.

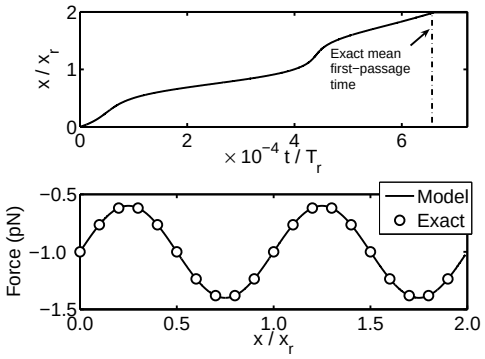

Figure 2.2: The first-passage time algorithm was validated by simulating a particle diffusing under the space-varying load $f(x) = -1+0.4\sin(2\pi x)$. The top plot shows the simulated path (solid) and the exact first-passage time (dashed) obtained by solving the Fokker-Planck equation directly and exactly. The bottom plot shows the exact and modeled forces. The reference space and time scales used in the plot are $x_r = 8$ nm and $T_r = 10^{-2}$ s.

2.1 Mathematical Description

Due to the small length scales of the problem, inertial effects are assumed negligible compared to the viscous forces which, hence, dominate the dynamics (46). Based on the sketch in Fig. 2.1, the equations of motion for the bead (b), strongly-bound head (s), and neck (n), are then

$$\gamma_b \dot{x}_b = -F_L + K_b\,(x_n - x_b)\,, \tag{2.1}$$

$$\gamma_s \dot{x}_s = K_s\,(u - x_s) + K_h\,(\Psi_s - \psi_s)\,, \tag{2.2}$$

$$\gamma_n \dot{x}_n = -K_b\,(x_n - x_b) - K_h\,(\Psi_s - \psi_s) - K_h\,(\Psi_w - \psi_w)\,, \tag{2.3}$$

where the subscript w refers to the weakly-bound head, $\psi_s = x_s - x_n$ and $\psi_w = x_w - x_n$, γ is the damping coefficient due to viscosity, $\dot{x}$ represents the velocity, x represents the position, u is the position of the binding site, F_L is the external load, K_b is the stiffness of the domain connecting the bead and the motor (cargo linker), K_h is the stiffness of the domain connecting a head to the neck (neck linker), and K_s is the spring constant representing the strong affinity to the microtubule in the

bound state. The distances Ψ_s and Ψ_w designate the equilibrium position of the neck with respect to the heads (when the internal strain is zero), while ψ_w and ψ_s designate the current position of the weakly-bound and strongly-bound heads.

The motion of the diffusing head is modeled using the average time for a particle to diffuse to a target in a given potential. The resulting forces on the diffusing, weakly-bound head (denoted by the subscript w) are caused by the potentials for the internal stresses (denoted by the subscript i) and the affinity to the microtubule (denoted by the subscript a), which may be expressed as

$$V_i(\psi) = \frac{1}{2}K_h\left(\Psi_w - \psi\right)^2, \tag{2.4}$$

$$V_a(x) = \begin{cases} F_w\frac{L_a}{\pi} - F_w\frac{L_a}{\pi}\cos\left[\pi\frac{(u-x)}{L_a}\right], & \text{if } |x-u| < L_a \\ 0, & \text{otherwise} \end{cases}, \tag{2.5}$$

so that

$$F_i(\psi_w) = K_h\left(\Psi_w - \psi_w\right), \tag{2.6}$$

$$F_a(x_w) = \begin{cases} F_w\sin\left[\pi\frac{(u-x_w)}{L_a}\right], & \text{if } |x_w-u| < L_a \\ 0, & \text{otherwise} \end{cases}, \tag{2.7}$$

where F_w is the affinity strength [pN] and L_a is the length [nm] over which the weak binding forces are active. The particular form of the second term in Equation 2.5 is chosen as a cosine function for convenience. This functional form leads to an attracting force at close distances from the binding site and zero force at large distances. Other functional forms that have a similar physical behavior can be used with a very small (negligible) effect on the overall results. Given the potentials in Equation 2.4 and 2.5, the complete potential for the diffusing head is

$$V = V_i(\psi_w) + V_a(x_w). \tag{2.8}$$

However, the forces acting on the diffusing head can vary in time due to unsteady forces on the bead. Consider the time instant t for the motor motion. The potential that each head has encountered until time t and position x is known. The potential of the diffusing head for the remaining distance to the binding site is estimated based on the current motor configuration and the potentials in all its domains. Using the known (past) and estimated (future) potentials, an estimated mean first-passage time for the diffusion between binding sites is calculated. This mean first-passage time is given by

$$t_0 = \frac{1}{j_0} = \frac{1}{D}\int_0^{x_0} \exp\left[\frac{-V(x)}{k_B T}\right]\left(\int_x^{x_0} \exp\left[\frac{V(y)}{k_B T}\right] dy\right) dx, \tag{2.9}$$

where D is the diffusion coefficient, x_0 is the distance between adjacent *free* binding sites ($x_0 = 16$ nm), k_B is the Boltzmann constant, and T is the absolute temperature (5, 46). Using t_0, one may then calculate the average velocity for the head to reach the next free binding site (at the estimated first-passage time) as

$$\dot{x}_w = \frac{x_0 - x}{t_0 - t}. \tag{2.10}$$

When the time interval between each re-estimation of the varying loads and corresponding potentials decreases, this algorithm converges to the *exact* mean first-passage time because the estimated potential converges to the exact potential as the head progresses. Compared to a kinetic approach, this method effectively considers forward and backward rates of the diffusion between binding sites, by considering the actual potential in which the head diffuses. However, once the head reaches the forward binding site, this method assumes that it binds irreversibly.

The heads are assumed to always be in opposite structural states. Thus, one chemical variable is used to describe the structural state of both heads. The switching of chemical, or nucleotide, states is assumed to be dependent on the configuration

of the motor and also on the ATP concentration (denoted by [ATP]). Before the diffusing head reaches the binding site, the chemical state variable is approximately constant. Once the diffusing head is within 1% of the distance to the binding site, the rate of change is given by

$$\dot{\rho} = \pm \frac{V_{\max}[ATP]^*}{K_M + [ATP]^*}. \tag{2.11}$$

To our knowledge, there is no available data for establishing the accuracy of the estimate of 1% of the distance between binding sites (0.08 nm). However, the overall results are only very weakly dependent on this parameter of the model. The asterisk denotes that [ATP] is measured in μM. We assume that each head follows Michaelis-Menten kinetics, defined by one reversible reaction followed by an irreversible reaction as follows,

$$E + S(K + ATP) \underset{k_{1b}}{\overset{k_{1f}}{\rightleftharpoons}} ES(K \cdot ATP) \xrightarrow{k_{2f}} P + E(K + ADP + Pi), \tag{2.12}$$

where E denotes enzyme, S denotes substrate, and P denotes product. The parameters $V_{\max}$ and K_M are defined as

$$V_{\max} = k_{2f}[E]_t, \tag{2.13}$$

$$K_M = \frac{k_{1b} + k_{2f}}{k_{1f}}, \tag{2.14}$$

where $[E]_t$ is the total enzyme concentration. The rates are defined as

$$k_{1f} = k_{1f,0}, \tag{2.15}$$

$$k_{1b} = k_{1b,0} \exp\left[\frac{\frac{1}{2}\kappa \left|\psi_s - \Psi_c\right|^{n_c}}{k_B T}\right], \tag{2.16}$$

$$k_{2f} = k_{2f,0}, \tag{2.17}$$

where $k_{1f,0}$, $k_{1b,0}$, $k_{2f,0}$,Ψ_c,n_c, and κ are parameters of the model. The molecule configuration (and implicitly the potentials and stresses in each of its domains) influences

the chemical kinetics by changing the effective k_{1b}. If a configuration, represented by ψ_s, is not at the optimal value for the chemical kinetics, then the backward rate increases, inhibiting the chemical transition. The optimal configuration is expressed through the reference angle, Ψ_c. Block et al. (11) and Carter and Cross (17) showed evidence that moderate assisting loads increase kinesin velocity, while the velocity decreases under large assisting loads, supporting the idea that an ideal stress state exists where the chemical reaction in Equation 2.12 is fastest. Note that in the absence of ATP, $\dot{\rho}$ is also zero.

The chemical state variable is considered to grow or decay until it reaches ± 1, at which time the nucleotide state of both heads switch. The chemical state variable describes the chemical state of a kinesin head (i.e. the nucleotide and MT-binding state of a particular head). The chemical state of a head, say A, is assumed to be unchanged until the chemical state of the other head, say B, switches. Before the switch, the chemical state variable characterizes the chemical kinetics of the head B. Once the head B switches, at that instant and until the next switch occurs, the chemical state variable characterizes the head A. The process repeats when the head A switches, and the chemical state variable once again characterizes the head B. The values between ± 1 for the chemical state variable may be interpreted as intermediate chemical conditions, but the specific values are not essential. The only role of the chemical state variable is to *predict the switching instants*, and account for the dependence of the time duration between consecutive switches on the stresses in the molecule. Hence, head to head coordination is assumed, requiring one variable rather than two. Moreover, the value of 1 for the switching condition was chosen for convenience. Identical results could be achieved with other values than 1 by simply scaling the constants $k_{1f,0}$, $k_{1b,0}$, and $k_{2f,0}$.

From a computational perspective, an integrator suited for nonsmooth (hybrid) systems is used for time marching and to solve for the switching times and states to machine precision. The dependence of the chemical kinetics on configuration is accounted for by using only the quantity ψ_s, i.e. the chemical kinetics are dependent on the instantaneous position of the bound head. This approach is capable of modeling exactly other more general dependencies because one may show that a dependence on ψ_s is in fact equivalent to a dependence on the location of *both* heads, given the structure and mechanical energy storage used in this model.

2.2 Parameter Values

The values for parameters were chosen from first physical principles and current experimental data regarding the structure of kinesin and microtubules. For example, the distance between binding sites is 8 nm, as in microtubules. Damping coefficients were estimated via Stokes' Law for a sphere, that is,

$$\gamma = 6\pi\zeta r, \tag{2.18}$$

where γ is the damping coefficient, ζ is the viscosity, and r is the radius of the sphere. The diffusion coefficient is then given through the Einstein relation, $D\gamma = k_B T$, where D is the diffusion coefficient, k_B is the Boltzmann constant, and T is the temperature. The size of a kinesin motor domain (head) has been estimated to be $4.5 \times 4.5 \times 7$ nm^3 (46). Therefore, we approximate the motor domain as a sphere of diameter 6 nm. The neck diameter was estimated as 2 nm. The model presented herein does not include internal friction (8). We assume that the motor protein can be approximated as globular domains that are elastically coupled. While this is an approximation, it provides a compromise between the accuracy of the predictions and the complexity of the model. Internal friction could be included in

the model by estimating its effects on the diffusion coefficients, or by adding another term to the potential. The affinity of the motor to the microtubule is estimated based on a phenomenological understanding of energies during the kinesin movement. Specifically, using the kinetic mechanism given in (21) for an ADP concentration of 20 μM, the change in free energy corresponding to weak binding was calculated to be 1.3 k_BT. The change in free energy corresponding to weak binding in this model is given by

$$\Delta E_w = \int_0^{L_a} F_a dx = \frac{2F_w L_a}{\pi}, \tag{2.19}$$

where L_a is the length over which the weak affinity is assumed to be active, and F_a is the force on the diffusing head due to affinity as shown in Equation 2.5. We assumed that L_a is 10% of the distance between binding sites (0.8 nm). Thus, a value of 5 pN for F_w (and 10 pN·nm for ΔE_w) results in an equivalent change in energy for weak binding. The mechanism in Cross (21) indicates that the change in free energy for strong binding is approximately 3.8 k_BT. If we assume that the maximum movement of the head while strongly bound is 0.1 nm, then K_s must be greater than $3 \cdot 10^3$ pN/nm for an equivalent change in energy. Thus, K_s was chosen to be 10^4 pN/nm. We note, however, that the values of F_w and K_s do not affect the force-velocity curves appreciably, provided K_s is greater than 500 pN/nm. Also, the steady-state force-velocity curve is entirely independent of the elasticity of the cargo linker (i.e. K_b).

The remaining parameters - that is the stiffness K_h, the equilibrium configuration $\psi_s = -\psi_w$, the chemical rate dependence on motor configuration and ATP concentration $k_{1f,0}$, $k_{1b,0}$, $k_{2f,0}$, κ, and Ψ_c - were solved for by using a Levenberg Marquardt optimization. The model was fit to two sets of experimental data (11, 105). Both sets of experimental force-velocity data were measured using a force-clamp optical

Parameter	(105)	(11) a	(11) b	Units
K_h	6.34	7.23	6.09	pN / nm
F_w	5	5	5	pN
K_s	10^4	10^4	10^4	pN / nm
L_a	0.8	0.8	0.8	nm
K_b	1	1	1	pN / nm
Ψ_s	0.437	1.40	1.71	nm
Ψ_w	-0.437	-1.40	-1.71	nm
Ψ_c	-3.66	-6.50	-8.37	nm
n_c	2	2	4.94	
$k_{1f,0}$	52.5	53.47	50.37	μM s^{-1}
$k_{1b,0}$	$3.69 \cdot 10^3$	$2.94 \cdot 10^3$	$3.28 \cdot 10^3$	s^{-1}
$k_{2f,0}$	$3.87 \cdot 10^-4$	$3.49 \cdot 10^-4$	$3.47 \cdot 10^-4$	s^{-1}
κ	3.73	1.63	1.06	pN / nm

Table 2.1: Parameter values for the mechanistic model obtained by fitting the model to experimental data in Visscher et al. (105) and Block et al. (11).

trap, and the data from Block et al. (11) includes assisting loads. The values for the parameters obtained are shown in Tab. 2.1. The values for several of the parameters ($K_h,\ k_{1f},\ k_{1b},\ k_{2f}$) are similar for the two experimental data sets. However, the fit to assisting load data required the parameter n_c to vary in the optimization, which then affected the values of $\Psi_s,\ \Psi_w,\ \Psi_c,$ and κ.

2.3 System Identification

Using the parameter values in Tab. 2.1 obtained from the experimental data of Visscher et al. (105), the resulting potential in which a head diffuses during one mechanochemical cycle is shown in Fig. 2.3. This potential was computed for a molecule in steady-state motion, under a constant load. The affinity of the weakly-bound head to the binding sites is evident in the potential wells at $x = 0$ nm and $x = 16$ nm, which correspond to the affinity of the head to the binding sites while the head is in the weakly-bound state. The general U-like shape of the potential is a result of the internal stresses. First, the internal stresses of the molecule propel the head forward, resulting in a downward slope in the potential. For the remaining

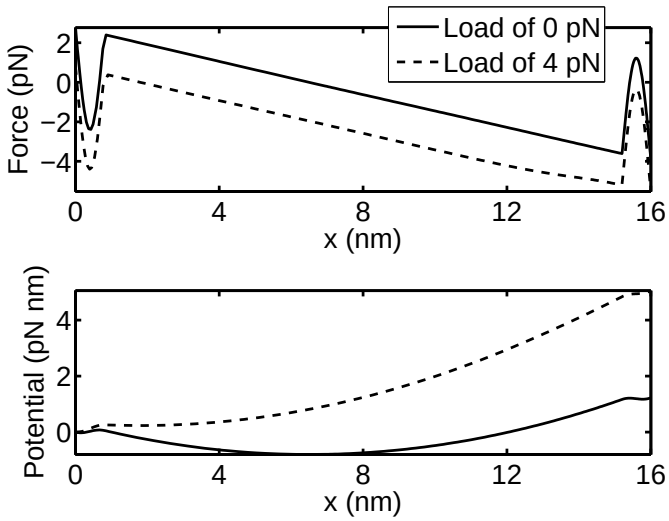

Figure 2.3: The potential of the diffusing head changes with load.

distance, thermal motion must work against the internal stresses of the molecule, as shown by the upward slope in the potential. The equilibrium position of the diffusing head, where the internal stresses balance, is the location where the derivative of the potential is zero. At zero load, the equilibrium position is approximately 2 nm behind the bound head. As the load is increased, the equilibrium position moves rearward.

Implications of the potential shown in Fig. 2.3 are evident in the average motion of the motor shown in Fig. 5.1. Specifically, the gradient of the potential is negative while the head is moving toward the equilibrium position. For this part of the motion, the head is being pulled forward by the internal stresses, and the motion is fast. Past the equilibrium position, the gradient of the potential is positive, indicating that diffusion must work against the internal stresses of the molecule, and the motion is slow.

In the mechanistic model, the mechanochemical cycle of the motor exhibits two distinct stages. During part of the cycle, alternating heads diffuse to the next unoccupied binding site. The remaining, and usually dominant, part of the cycle consists

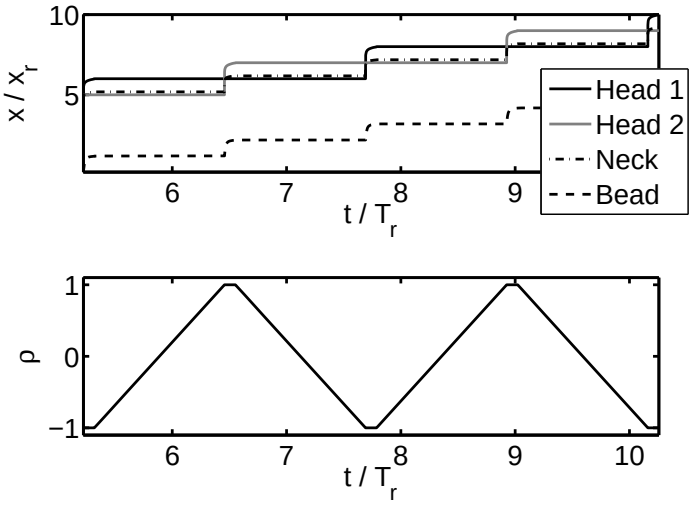

Figure 2.4: The dynamics of the motor under a load of 4 pN and ATP concentration of 2 mM. The top plot shows the heads, neck and bead motion. The bottom plot shows the time variation for the chemical state variable ρ. The reference space and time scales are $x_r = 8$ nm and $T_r = 10^{-2}$ s..

of the motor being almost stationary, waiting for the chemical reaction to proceed. The chemical reaction is highly dependent on ATP concentration, while diffusion is not. Thus, the diffusion ratio r_d was defined to explore how the ratio of time spent diffusing to the time waiting for the chemical reaction to proceed depends on ATP concentration. The diffusion ratio, is defined as

$$r_d = \frac{\tau_d}{\tau_c} = \frac{\text{diffusion time}}{\text{chemical time}}, \tag{2.20}$$

where τ_d is the time for the free head to diffuse to the next binding site, and τ_c is the time for the chemical reaction at the head to occur and change the structural state. The diffusion ratio changes with load and ATP concentration as seen in Fig. 2.5. The diffusion ratio influences the shape of the force-velocity curve. A low r_d corresponds to a concave force-velocity curve, while a high r_d results in a convex curve.

The ability to fit well the force-velocity relationship of kinesin over a large range of loads and ATP concentrations is an important feature of the model. Using one

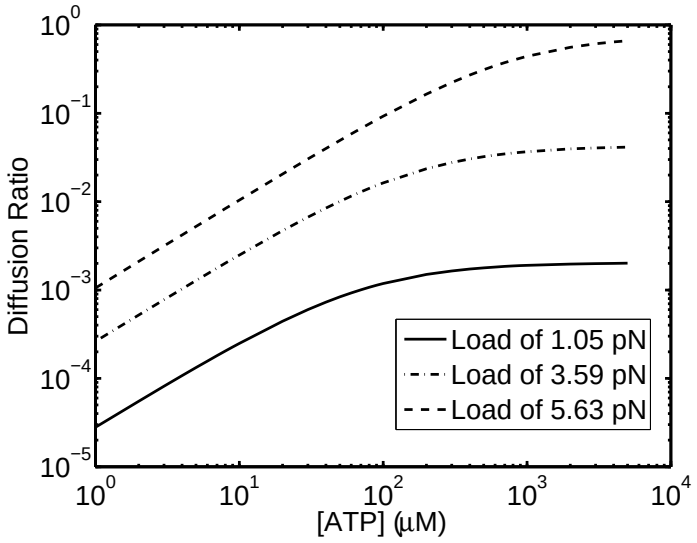

Figure 2.5: The diffusion ratio influences the shape of the force-velocity curve.

set of parameters, the model is able to capture the force-velocity behavior of kinesin, as seen in Figs. 2.6 and 2.7. The proposed model is able to capture the changes in the shape of the force-velocity curve not only at a fixed ATP concentration, but also over a large range ATP concentrations. We note that the results presented are for *constant* values of the parameters, although the motor conditions changed dramatically, e.g. ATP concentration varied over more than 4 orders of magnitude.

Two recent experiments examined kinesin under assisting loads (11, 17). The data

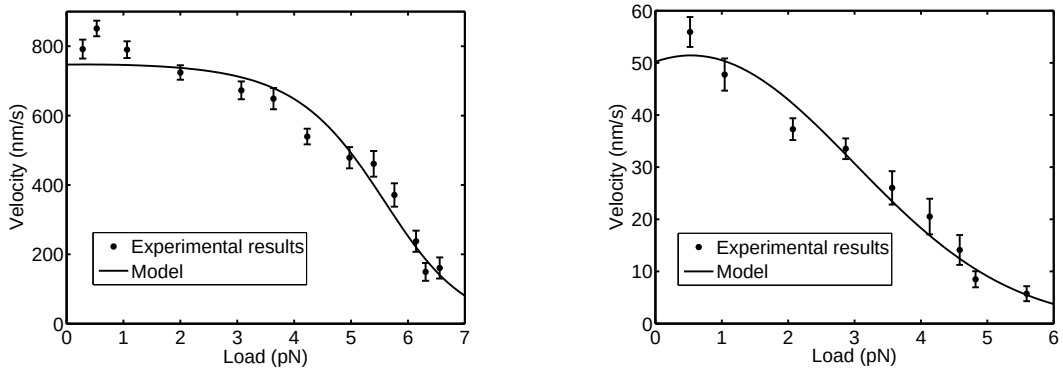

Figure 2.6: The results of the model closely match the force-velocity data from Visscher et al. (105) for various ATP concentrations: 2 mM (left) and 5 μM (right).

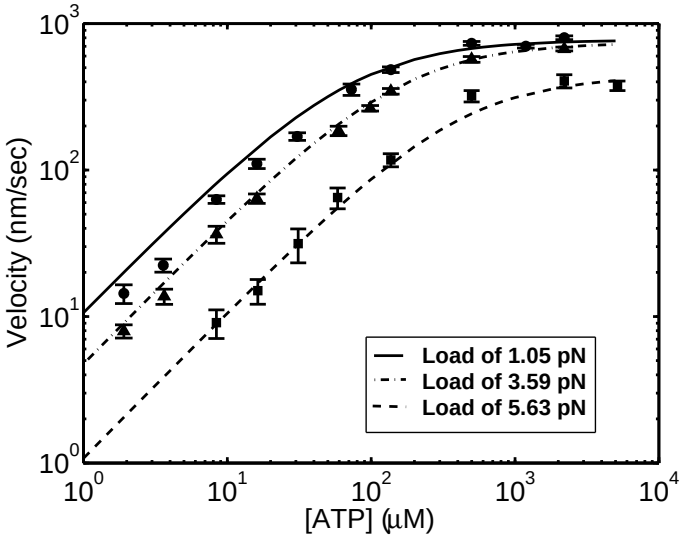

Figure 2.7: The ability to describe very well the force-velocity relationship of kinesin over a large range of loads and ATP concentrations is an important feature of the model. Model predictions for a large range of ATP concentrations are shown by lines, while experimental force-velocity results from Visscher et al. (105) are shown by symbols.

of Block et al. (11) suggests that moderate assisting loads increase velocity while the velocity saturates under high assisting loads. Conversely, the data of Carter and Cross (17) suggests moderate assisting loads (< 7 pN) increase velocity, but the velocity then decreases under high assisting loads (> 7 pN). The force-velocity under assisting loads provides insight into the stress dependence of the chemical reaction. Using a value of 2 for n_c, shown by fit (a) in Fig. 2.8, the model fits the majority of the data from (11) well, but does not fit a single data point at high assisting loads. However, the results for $n_c = 2$ were included because they show a behavior similar to the data of (17). When the parameter n_c is allowed to vary in the optimization, the model is able to fit all of the data well as shown in Fig. 2.8, for fit (b).

A crucial aspect of any model of molecular transport is its capability to provide insights into the physical phenomena governing the dynamics. In particular, understanding how various physical parameters in the model affect the force-velocity and

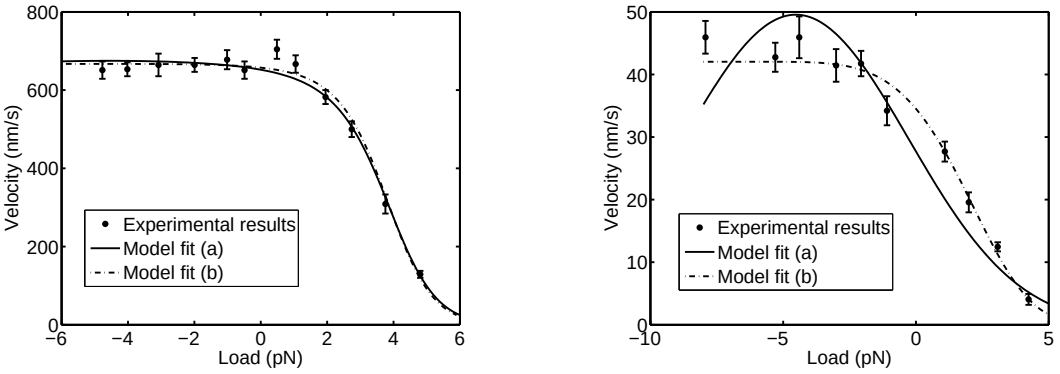

Figure 2.8: The results of the model closely match the force-velocity data from Block et al. (11), for various ATP concentrations: 1.6 mM (left) and 4.2 μM (right).

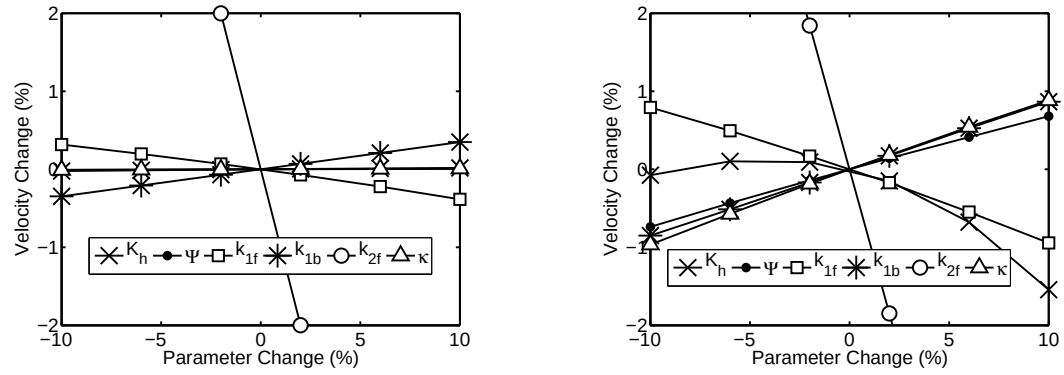

Figure 2.9: The sensitivity of the force-velocity curve to model parameters.

transient physical dynamics is of great interest. Fig. 2.9 shows the sensitivity of the predicted velocity to several model parameters. Note that the predicted velocity is sensitive to k_{2f} at low loads, where diffusion is fast compared to the chemical reaction. At moderate loads, where diffusion is much slower, the predicted velocity is sensitive to all parameters, while k_{2f} remains dominant. The parameters whose sensitivity is load-dependent affect the shape of the force-velocity curve. For instance, increases in κ, Ψ, and k_{1b} do not have a large effect on velocity at low loads, but increase velocity at moderate loads, resulting in a more convex force-velocity curve. Similarly, increasing k_{1f} and K_h results in a more concave force-velocity curve.

CHAPTER III

Monte Carlo Simulations

In the previous chapters, a deterministic model was presented that describes the mean behavior of a stochastic process. To validate that the deterministic model accurately predicts the mean behavior, and to investigate any significant realizations away from the mean, Monte Carlo simulations were performed. The parameters and equations were the same as in the mechanistic model with three important exceptions. In the mechanistic model, the diffusion is modeled through the mean first-passage time. In the Monte Carlo simulation, the forces due to diffusion are modeled directly through random variables, such that the equations for x_s, x_w, x_h and x_b are in the form

$$\gamma \dot{x_j} = -\frac{\partial V_j(t)}{\partial x} + \Gamma_j(t), \tag{3.1}$$

where the mean $< \Gamma_j(t) >= 0$ and the auto-correlation $< \Gamma_j(t), \Gamma_j(t') >= 2\gamma k_B T \delta(t - t')$ with δ being the delta function (82). The subscript j stands for $s,\ w,\ n$, and b, respectively. A random component is also added to the chemical kinetics, such that

$$\dot{\rho} = \pm \frac{V_{\max}[ATP]^*}{K_M + [ATP]^*} \cdot \frac{1}{\Gamma_\rho}, \tag{3.2}$$

where Γ_ρ is gamma-distributed (1, 27, 63, 74). Also, the mechanistic model assumes that the external force on the bead due to the optical trap (used experimentally to

apply a load (11, 17, 60, 97, 102, 105)) is constant. The Monte Carlo simulation models the optical trap as a linear spring between the bead and the center of the optical trap. The center of the optical trap is updated based on a moving average of the bead location, as is done in experiments. Fig. 3.1 shows a typical realization of the Monte Carlo simulation. Fig. 3.2 shows the distribution of the diffusion times and chemical times for 250 steps of a single motor under an average load of 1.91 pN. The diffusion time distribution is exponential, as expected for a waiting-time phenomena. The chemical time follows a gamma distribution, as was expected. The mean velocity, 740 nm/s, agrees well with the mean velocity of 739 nm/s predicted by the mechanistic model.

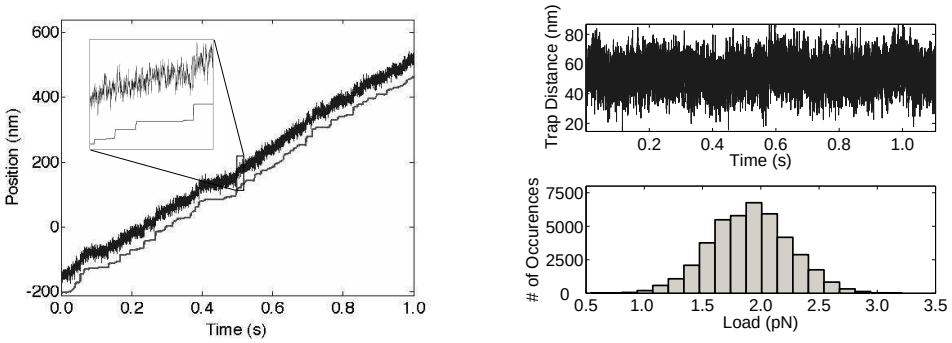

Figure 3.1: The trap location (wide gray line) is updated based on a running average of the bead location (thin black line) such that the load is approximately constant.

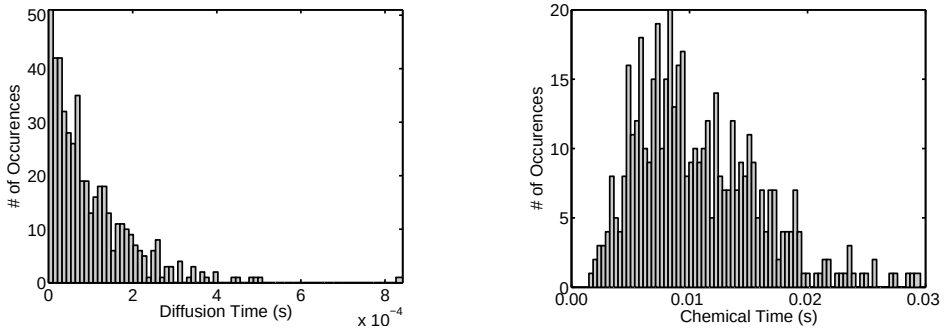

Figure 3.2: The diffusion time (left) is exponentially distributed while the chemical time (right) is gamma distributed.

CHAPTER IV

Single Motor Dynamics

The transient description herein allows many observations into the underlying dynamics of kinesin. To study how a single motor (interpreted as an oscillator) responds to time-varying forces, the load was varied sinusoidally over a range of frequencies. The significant changes in the average velocity of the dynamic response (over 100 cycles) due to the fluctuating excitation shows that transients are likely to play a significant role in kinesin movement. Fig. 4.1 shows the frequency response in terms of average velocity of the dynamic response (over two periods of the excitation). As shown, the cargo linker stiffness K_b affects the transient response of the motor/cargo. Experiments to test these predictions could be performed by changing the cargo linker stiffness similar to the approach used by Jaud et al. (52) to modify the neck linker stiffness. The quasi-steady frequency response was calculated by assuming the instantaneous velocity was equal to the velocity from the steady-state force-velocity curve, i.e. where transients are assumed negligible. As shown in Fig. 4.1, the quasi-steady result accounts for the initial drop in average velocity with a time-varying load. This is due to the nonlinearity in the force-velocity curve, i.e. an increase in load has a much greater effect on the velocity than a decrease in load. The frequency response shows variations in the average velocity of up to 400 nm/s

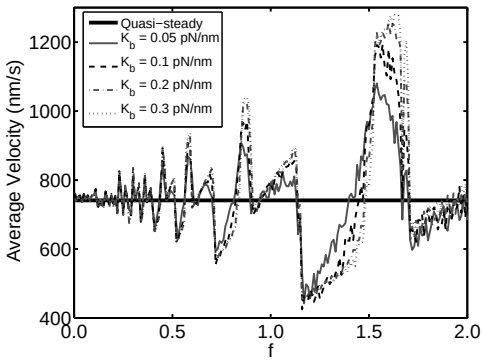

Figure 4.1: The response in average velocity to the excitation frequency is affected by the cargo linker stiffness. The load is of the form $f(t) = 2 - 2\sin[2\pi(0.01f)t]$ and [ATP]=2 mM.

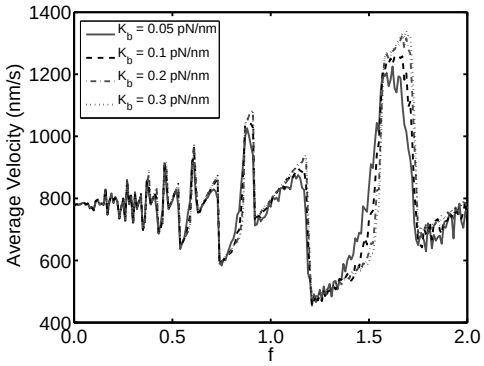

Figure 4.2: The response in the average velocity of *two* motors to the excitation frequency is affected by the cargo linker stiffness. The load is of the form $f(t) = 2 - 2\sin[2\pi(0.01f)t]$ and [ATP]=2 mM.

beyond the quasi-steady variation, illustrating that transient dynamics are indeed significant.

Transient effects are also likely to affect motor cooperativity. To demonstrate this, Fig. 4.2 shows the response of the average velocity of two coupled motors to the frequency of the time-varying load. Resonances are shifted to slightly higher frequencies for all values of the cargo linker stiffness. The frequency response is also shifted to higher velocities, about 50 nm/s on average.

CHAPTER V

Collective Dynamics of Motors with Deterministic Chemical Kinetics

Much attention has been paid to understanding the molecular mechanism of force generation by single-molecule experiments using various molecular motors, most notably kinesin-1 and myosin-V (7, 29, 31, 54, 59, 78, 86). Considerably less work has focused on the effect of coupling among multiple motor proteins, despite considerable evidence that many motor proteins function collectively in cells (37, 39, 99). Herein, we use a transient model to explore the implications of cooperativity between multiple motors. An understanding of collective motor dynamics provides a link between in vitro, single molecule experiments and the mechanisms of kinesin in the cell. Coupled motors can experience time-varying loads at time scales faster that their stepping frequency due to coupling through a common cargo, unless the motors are perfectly synchronous. Thus, a dynamic model capable of capturing transients is needed to accurately describe the interaction of the two head domains in a single kinesin motor molecule and interactions among several motor proteins. Previously, we developed a *transient, deterministic* model using a novel approach based on an approximation of the kinesin-1 geometry and the mean first-passage time (44). Herein, we use the mechanistic model to study the dynamics of multiple kinesin-1 motors coupled through a shared load. Several novel metrics, tailored to analyze

the behavior of molecular motors viewed as coupled nonsmooth oscillators are introduced. Molecular motors are nonlinear due to the nonlinear relationship between external force and velocity on diffusion and the chemical kinetics. Molecular motors are nonsmooth due to the discontinuities in the dynamics caused by the conformational change. A parametric study of the dynamics of two coupled motors is shown to illustrate these metrics.

When multiple motors pull a common cargo, the model assumes that the motors cannot sterically interfere with one another or their binding sites. This is equivalent to assuming that the attachment points to the cargo are adequately spaced so that the motors will not interfere with one another while they are mechanically coupled. Therefore, the only coupling between the motors is through the load. Also, the cargo linker is assumed to sustain only forces in tension, not compression. Thus, for N coupled motors the equations for the necks and common cargo are,

$$\gamma_n \dot{x}_{n,k} = -F_{b,k} - K_h \left(\Psi_s - \psi_{s,k}\right) - K_h \left(\Psi_w - \psi_{w,k}\right), \tag{5.1}$$

$$\gamma_b \dot{x}_b = -F_L + \sum_{k=1}^{N} F_{b,k}, \tag{5.2}$$

where

$$F_{b,k} = \begin{cases} K_b \left(x_{n,k} - x_b\right), & \text{if } \; x_{n,k} - x_b > 0 \\ 0, & \text{otherwise} \end{cases} . \tag{5.3}$$

5.1 Metrics of Synchronization

A large body of previous work on coupled oscillators has focused on simple, one degree-of-freedom oscillators (51, 67, 75, 79, 90, 93). However, motor proteins are nonsmooth oscillators with multiple time scales in the cycle. The nonsmoothness is caused by the switching in the variables Ψ_s and Ψ_w in Eqs. 2.1-2.3 and by the tether behavior of the cargo linker in Eq. 5.3. The multiple time scales are caused

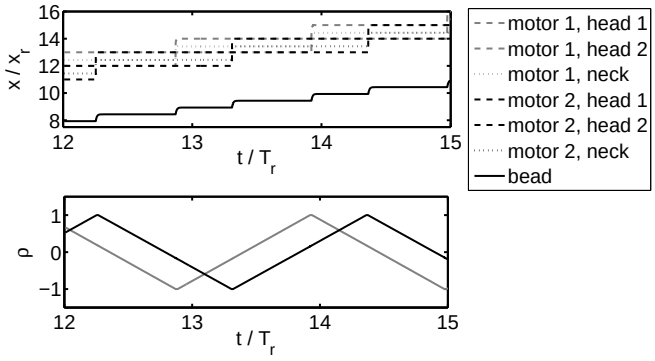

Figure 5.1: The dynamics of two motors under a load of 2 pN and ATP concentration of 2 mM. The bottom plot shows the chemical state variable. The reference space and time variables are $x_r = 8$ nm and $T_r = 10^{-2}$ s.

by the difference in average velocity during diffusion and during the dwell time as seen in Fig. 5.1. Accordingly, the novel metrics of synchronization discussed below are specifically tailored to nonsmooth oscillators.

5.1.1 Complex Order Parameter

A useful measure of synchronization for simple oscillators is the complex order parameter

$$re^{i\alpha} = \frac{1}{N}\sum_{j=1}^{N} e^{i\beta_j} \tag{5.4}$$

first proposed by Kuramoto (67). The oscillators are visualized as points traveling on the unit circle, where the complex order parameter is the centroid of the points. For example, if the oscillators are synchronized, the points are co-located on the unit circle at all times, so $r = 1$. If two oscillators have a phase difference of 180 degrees, they are at opposite locations on the unit circle at all times, so $r = 0$. This metric assumes that each oscillator j can be completely described by a phase β_j. The phase must be defined as an invertible function of the state such that each phase defines a unique state of the oscillator. Such a phase was defined for each motor in the

mechanistic model as follows,

$$\beta = \begin{cases} \frac{\pi}{2}(\upsilon + 1) + 2\pi(k-1), & \text{if head 2 is strongly bound} \\ \pi + \frac{\pi}{2}(1-\upsilon) + 2\pi(k-1), & \text{if head 1 is strongly bound} \end{cases}, \tag{5.5}$$

where $\upsilon = \frac{1}{2}(x_{\text{head 1}}/x_r - x_{\text{head 2}}/x_r + \rho)$, k is the cycle index and x_r is the length scale used (8 nm). During the cycle, $x_{\text{head 1}}/x_r - x_{\text{head 2}}/x_r$ varies monotically from -1 to 1. The variable ρ increases from -1 to 1 while head 2 is strongly bound, and decreases from 1 to -1 while head 1 is strongly bound. Therefore, each full cycle of the motor results in a phase increase of 2π and each phase value is invertible to a unique oscillator state. A typical example of the resulting complex order parameter for two coupled motors is shown in Fig. 5.2. The shape of the orbit of the order parameter in the complex plane changes corresponding to changes in the coupled oscillator dynamics. A Poincaré section (38) is taken when the angle of the complex order parameter (α) is equal to zero, i.e. the real part is positive and the imaginary part is zero. The section provides a metric for synchronization of the nonsmooth oscillators (r' denotes the Poincaré section of the complex order parameter), as shown in Fig. 5.3. In this example, the motors are initially at a desynchronized state. With increasing time, the coupling between the motors leads to a generalized phase-locked dynamics, i.e. there is a constant difference in phase between the motors $\Delta\beta$ each time $\alpha = 0.$, indicated by a constant r' in time. The interpretation of the complex order parameter is somewhat complicated by the particular dynamics of kinesin-1. Each cycle of the motor consists of two symmetrical steps, which means that kinesin-1 can be interpreted as a period-2 oscillator. For example, for two oscillators, a complex order value of zero corresponds to the oscillators being 180° out of phase. This state is dynamically identical to the synchronized state, except that head 1 of one motor is stepping at the same time as head 2 of the other motor. Due to this

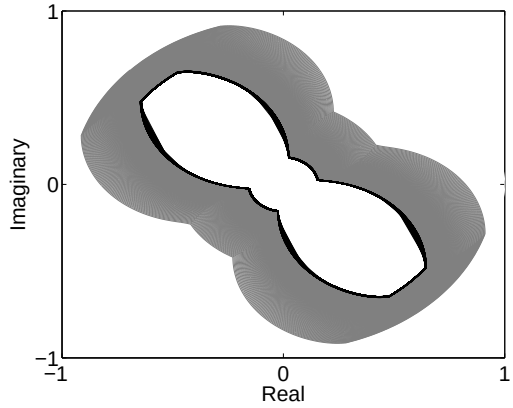

Figure 5.2: Complex order parameter for two coupled motors. The motor parameters are varied such that each motor has a slightly different intrinsic velocity.

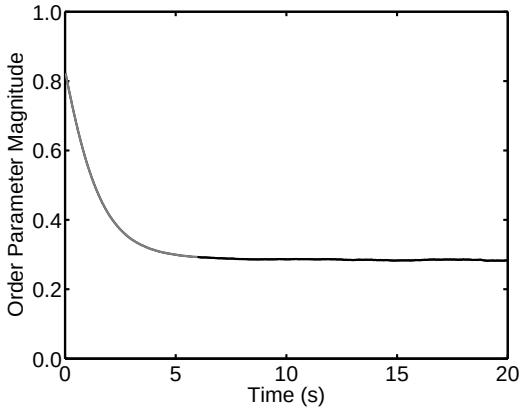

Figure 5.3: Poincaré section of the complex order parameter at $\alpha = 0$. The shades in the plot correspond to Fig. 5.2.

symmetry, complex order parameter values of zero and one both correspond to fully synchronized states.

5.1.2 Correlation Dimension

In addition to the complex order parameter, the dimensionality of the attractor of the dynamics in state space provides a measurement of the degree of synchronization. It is expected that when the oscillators are not synchronized, the trajectory in state space is complex and requires many coordinates to describe its evolution. Hence,

the dimensionality of the attractor of the dynamics is high. The maximum of the dimension is the total number of degrees of freedom. Conversely, if the oscillators are perfectly synchronized, the dynamics will lie on a simple attractor, which can be described by a unique coordinate, so that the attractor has a minimal dimension. For example, if the oscillators perfectly synchronized, the trajectory of the system of coupled molecular motors is a single limit cycle, and the dimensionality of the attractor will be one. The dimensionality is a particularly useful measure as it takes into account inherent symmetries in the system, e.g. the period-2 limit cycle behavior of the kinesin motors. Also, the dimensionality is an invariant of the dynamics, which remains unchanged irrespective of the coordinates used to describe the system. This is a feature particularly useful for comparing various sets of experimental or computational results in a consistent manner. In its usual definition, the dimensionality is calculated at steady state. However, we would like to characterize changes in the dimensionality of the attractor in time. Accordingly, we assume the time scale of changes in the dimensionality take place slowly relative to the dynamics of the system. Thus, the time series can be broken into intervals of sufficient length to calculate an approximate correlation dimension (35, 92). The trajectory is continuous, so the correlation dimension is calculated based on the length of the trajectory inside a given neighborhood, instead of on the number of points. This results in an efficient and accurate method of calculation. As shown in Fig. 5.4, the dimension decreases with increased synchronization of the oscillators so that a low dimension corresponds to a high degree of synchronization.

5.1.3 Phase Difference

The phase difference between motors is a useful measurement of synchronization. The phase β is compared for two motors. The time at which the difference between

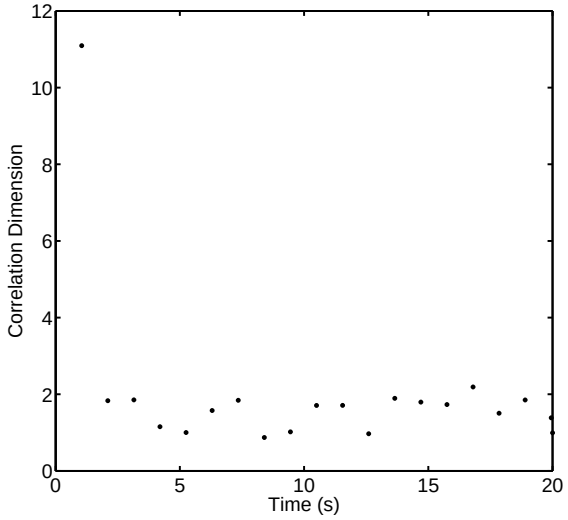

Figure 5.4: Correlation dimension for two coupled motors. The oscillators settle to an approximately phase-locked dynamics with slightly higher dimensionality than a limit cycle.

the two phases $\Delta\beta$ is minimized is defined as the phase difference between the two oscillators, Φ. When more that two oscillators are coupled, the phase difference is calculated between each motor and one motor chosen as the reference, and the mean of these phase differences is used. The physical meaning of Φ is the time lag (or lead if $\Phi < 0$) between two oscillators. For example, when two motors are phase locked onto a limit cycle, the value of Φ is constant in time. Fig. 5.5 shows the phase difference between the coupled motors. The motors are initially synchronized, thus $\Phi = 0$. The difference in intrinsic velocities between the motors then causes them to settle onto a phase-locked dynamics, i.e. the phase difference is constant in time.

The phase difference is also visualized through embedded coordinates (55). In this manner, we can search for fixed points in the phase difference, and analyze the stability of these fixed points. Here, the phase difference is used as the embedded coordinate. The choice of an appropriate value of the lag time, T, represents a compromise between a small value that results in the phase portrait being crowded around the diagonal and a large value that results in the phase portrait filling the

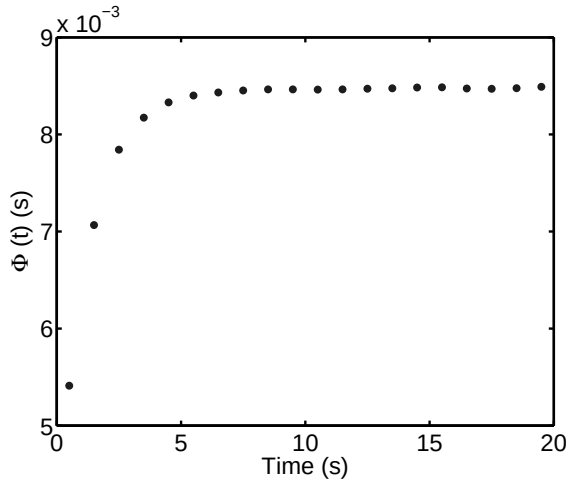

Figure 5.5: Phase difference for two coupled motors. The phase difference between the motors settles to a constant value.

phase space. The phase portrait of the phase difference for two coupled motors is shown in Fig. 5.6. As in the previous figure, the motors settle to a phase-locked dynamics, here shown as a fixed point in the phase portrait.

5.1.4 Energy Analysis

A method was developed to quantify the amount of energy in the phase-locked mode of coupled oscillators. Here, we use a definition for the modal energy in the dynamics like that used in proper orthogonal decomposition analysis. The average modal energy in the dynamics is defined, for a vector v, as

$$E = \frac{1}{T}\int_0^T \frac{1}{2}x(t)\cdot x(t)dt, \tag{5.6}$$

If x corresponds to a velocity, the average modal energy corresponds to the average kinetic energy. However, for states such as the chemical state variable, there is no physical corollary to the energy. Nonetheless, this definition of energy is useful when analyzing the dominant dynamics of a system. If the oscillators are phase-locked, or the phase difference between the oscillators is constant in time, the fraction of energy in the phase-locked mode to the total amount of energy in the dynamics is

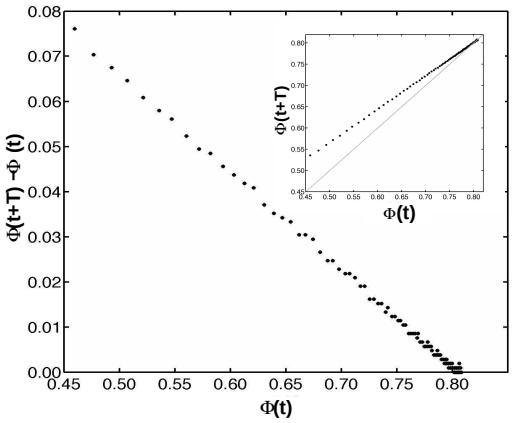

Figure 5.6: The phase portrait of the phase difference for two coupled motors in terms of the period of the limit cycle at steady state. The phase portrait is rotated 45 degrees from the standard depiction (shown in the inset) to allow for greater detail.

close to one. If the oscillators are not perfectly phase-locked, the fraction is lower. The energy-based method simultaneously solves for the phase difference between oscillators. The calculation proceeds as follows. First, a matrix is constructed of the values of the states of the system at many times

$$X = \begin{bmatrix} \bar{x}_1(t_1) & \bar{x}_1(t_2 & \cdots & \bar{x}_1(t_N) \\ \bar{x}_2(t_1) & \bar{x}_2(t_2 & \cdots & \bar{x}_2(t_N) \\ \vdots & \vdots & \ddots & \vdots \\ \bar{x}_M(t_1) & \bar{x}_M(t_2 & \cdots & \bar{x}_M(t_N) \end{bmatrix} \tag{5.7}$$

where $\bar{x}_m(t_n)$ denotes the states of oscillator m at time t_n. Each oscillator is then phase-shifted with respect to oscillator 1 such that

$$\begin{aligned} X(\bar{\tau}) &= \begin{bmatrix} \bar{x}_1(t_1) & \bar{x}_1(t_2) & \cdots & \bar{x}_1(t_N) \\ \bar{x}_2(t_1+\tau_1) & \bar{x}_2(t_2+\tau_1) & \cdots & \bar{x}_2(t_N+\tau_1) \\ \vdots & \vdots & \ddots & \vdots \\ \bar{x}_M(t_1+\tau_{M-1}) & \bar{x}_M(t_2+\tau_{M-1}) & \cdots & \bar{x}_M(t_N+\tau_{M-1}) \end{bmatrix} \\ &= \begin{bmatrix} X_1 & X_2 & \cdots & X_N \end{bmatrix} \end{aligned} \tag{5.8}$$

where $\bar{\tau} = [\tau_1, \tau_2, \cdots, \tau_{M-1}]$ is a vector containing the phase shift of each oscillator with respect to oscillator 1. The mode shape of the drift, the component of the dynamics due to the average velocity of the oscillators (i.e. when all states are moving together), is

$$D = [1,\ 1,\ \cdots,\ 1]^T . \tag{5.9}$$

We can then subtract the component of dynamics due to the drift and the mean

$$X'_n = X_n - \frac{D^T \cdot X_n}{D^T \cdot D} D \tag{5.10}$$

$$\tilde{X}_n = X'_n - \langle X'_n \rangle. \tag{5.11}$$

For the kinesin model, the states of each motor (oscillator) are defined as

$$\bar{x}_m = [x_{head1},\ x_{head2},\ x_{neck},\ \rho]^T \tag{5.12}$$

where the states are the position of head 1, the position of head 2, the position of the neck, and the chemical state variable. Thus, we define the mode shape of the synchronous motion for each motor as

$$\bar{s}_m = [1,\ -1,\ 0,\ 0]^T . \tag{5.13}$$

The mode shape of synchronous motion for the collection of oscillators is then

$$S = [\bar{s}_1\ \bar{s}_2\ \cdots\ \bar{s}_M] . \tag{5.14}$$

From the definition in Eqn. 5.6, the total energy in the dynamics is

$$E_{tot} = \frac{1}{2T_{tot}} \sum_{n=1}^{N} \Delta t \left(\tilde{X}_n^T \cdot \tilde{X}_n \right), \tag{5.15}$$

where $\Delta t = t_n - t_{n-1}$ and $T_{tot} = \sum_{n=1}^{N} \Delta t$. We now seek the component of the energy along the vector S, or the energy in the phase-shifted mode. The projection of $\tilde{X}_n$

along S is given by

$$\tilde{X}_n^{\parallel} = \frac{S^T \cdot X_n}{S^T \cdot S} S. \tag{5.16}$$

The energy in the phase-shifted mode is then

$$\begin{aligned} E_{ps}(\bar{\tau}) &= \frac{1}{2T_{tot}} \sum_{n=1}^{N} \Delta t \left[(\tilde{X}_n^{\parallel})^T \cdot (\tilde{X}_n^{\parallel}) \right] \\ &= \frac{1}{2T_{tot}} \sum_{n=1}^{N} \Delta t \frac{\left(S^T \cdot \tilde{X}_n\right)^2}{S^T \cdot S} \end{aligned} . \tag{5.17}$$

Finally, an optimization routine is used to find the time delays, $\bar{\tau}$, that correspond to the maximum energy in the phase-shifted mode. The optimization routine minimizes the cost function

$$C(\bar{\tau}) = 1 - \frac{E_{ps}}{E_{tot}}. \tag{5.18}$$

The cost function is shown as a function of the phase $\bar{\tau}$ for two coupled motor proteins in Fig. 5.7. As shown, if the cost function is minimum at τ, the function will also be minimum at $\tau + T$ where T is the period of the oscillator. Thus, we choose the phase where the magnitude of both τ and the cost function are minimum. The energy analysis results in the fraction of energy in the phase-locked mode and the phase between oscillators.

5.2 Collective Motor Dynamics

Considerable evidence implies that kinesin-1 motors operate collectively in cells, with several motors transporting a common cargo. In that context, the ability of the mechanistic model to handle transient dynamics makes it especially well-suited to modeling multiple motors, as coupling between motors introduces time-varying loads. Each time one motor steps, it influences the load on all the other motors. The only case where the load on the motors is constant is when all motors are perfectly

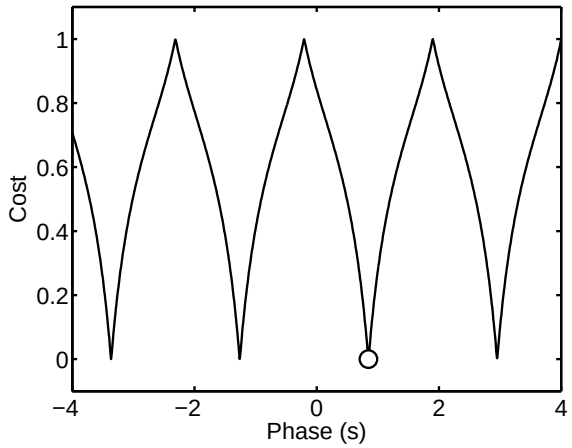

Figure 5.7: The energy in the phase-locked mode is maximum when the cost function is minimum.

synchronized, i.e. all motors are at the same point in their mechanochemical cycle at all times.

The central question is: how do groups of kinesin motors collectively transport a load? There are several possibilities. The motion of the motors may be uncorrelated as occurs when the coupling between motors is very weak and does not affect their motion. On the other extreme, the coupling may be very strong and cause the motors to be fully synchronized. In this case, the motors are all at the same point in the mechanochemical cycle at any given instant. An intermediate case is also possible and most likely, where the coupling between motors is moderate and they are not fully synchronized, but their influence on one another is significant. The motors may become phase-locked, where there is a constant phase difference between motors. Alternately, subgroups within the collection may become synchronized, but not the entire collection.

The mechanistic model allows us to investigate how model parameters (e.g. linker stiffness, chemical kinetics) and conditions (e.g. load and ATP concentration) effect the collective behavior of multiple, coupled motor proteins. Using metrics of syn-

chronization tailored for use with nonsmooth oscillators, a parametric study was conducted to observe the effect of model parameters on the synchronization and efficiency of two coupled kinesin motors. The two motors were assumed to have slightly different chemical kinetics, implemented through a variation of k_{1f}. As described previously, let us denote the Poincaré section of the complex order parameter when $\alpha = 0$ as r'. In the mechanistic model, one mechanochemical cycle includes two steps of the motor. For two motors, this symmetry results in fully synchronous dynamics at $r' = 0$ and at $r' = 1$. The efficiency of the transport was calculated as

$$\eta_P = \frac{\text{mechanical energy}}{\text{chemical energy}}, \tag{5.19}$$

where the energy was calculated over the mechanochemical cycle. The chemical energy over one cycle assumes that one molecule of ATP is hydrolyzed per each step (8 nm advance) of the motor. The mechanical energy is the integral of the mechanical power (the force exerted by the motor times the velocity of the motor) over the mechanochemical cycle. For each parameter set, the motors were started in a synchronized state. Then, the simulation was advanced 1000 mechanochemical cycles (2000 steps) to insure the dynamics reached steady state.

5.2.1 Effects of the Cargo Linker Stiffness

The cargo linker stiffness (K_b) affects the strength of the coupling between motors. A range of cargo linker stiffnesses was examined for a constant load (2 pN) and a fixed standard deviation ($\text{std}(k_{1f}) = 6\ \mu\text{Ms}^{-1}$). Fig. 5.8 shows the effect of cargo linker stiffness on efficiency, average velocity, order parameter, correlation dimension, and phase difference. Overall, the efficiency increases with increased stiffness, or increased coupling strength. However, there is a local optimum around $K_b = 0.5$ pN/nm. As discussed in section 5.1.1, the Poincaré section of the complex order parameter is

shown. If K_b is less than 0.5 pN/nm, r' oscillates, even at long times (2000 steps). For these cases, the value of r' in the Poincaré section holds little meaning. If K_b is greater than 0.5 pN/nm, r' reaches a constant value, implying a phase-locked state. A synchronous state exists at $r' = 0$. Thus, the local maximum of the efficiency at $K_b = 0.5$ pN/nm corresponds to a near-synchronous state at this condition, as the order parameter is constant in time, and approaches a value of zero. The efficiency is again high as the motors approach a synchronous state at high values of K_b, where r' is near 1. A similar trend is shown by the correlation dimension, where at low values of K_b, the dimension is high, indicating a low degree of synchronization. At $K_b > 0.3$, the correlation dimension settles around a value of 1.8, indicating a high degree of synchronization. Similarly, the phase difference decreases with increasing coupling strength.

By viewing the phase difference in embedded coordinates, the stability of the synchronized state can be analyzed. As shown in Fig. 5.9, stronger coupling through larger values of K_b causes the fixed point to become more stable, as evidenced by the decreased slope of the phase portrait. The phase portrait at each condition becomes steep as it nears the fixed point, because when the motors are close to a synchronized state, they diffuse during the same time which increases their interaction.

5.2.2 Effects of the Load

The load on the motors affects the synchronization of the motors as well, as shown in Fig. 5.10. The efficiency of the motors increases with increasing load, as the mechanical work is larger for larger loads. One would expect the steady-state average velocity to decrease with load. However, the velocity is largest at a load of 3 pN, due to the motors synchronizing at this condition. Interestingly, the degree of synchronization also increases with load. This result follows the trend shown by

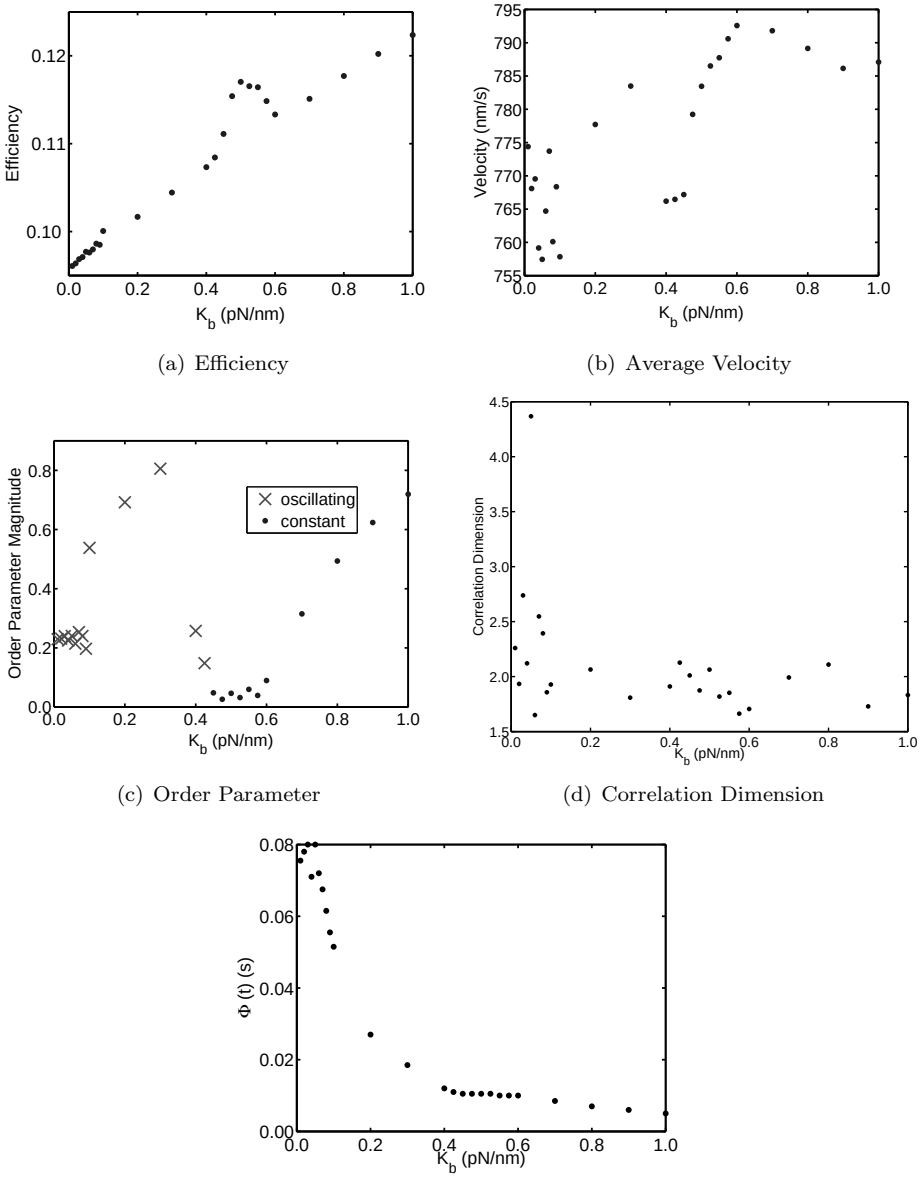

(a) Efficiency

(b) Average Velocity

(c) Order Parameter

(d) Correlation Dimension

(e) Phase Difference

Figure 5.8: The effect of the cargo linker stiffness (K_b) on the synchronization. The difference in instrinsic velocity and load were constant (std(k_{1f}) = 6 μMs^{-1}, Load = 2 pN).

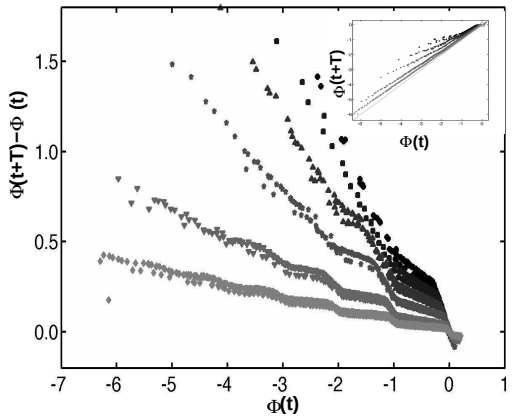

Figure 5.9: The effect of the cargo linker stiffness on the phase portrait of the phase difference for two identical coupled motors: K_b = (♦) 0.1 pN/nm, (▼) 0.2 pN/nm, (★) 0.4 pN/nm, (▲) 0.6 pN/nm, (■) 0.8 pN/nm, (•) 1.0 pN/nm.

varying cargo linker stiffness, that an increased degree of synchronization results in increased efficiency. The utility of the correlation dimension is demonstrated here, as at loads greater than 7 pN, the order parameter is approximately constant at a value of one, indicating a synchronized state. However, the correlation dimension shows that the degree of synchronization varies at loads greater than 7 pN. These details are not shown by the order parameter as it is a Poincaré section, only giving information at one point in the cycle. Overall, the results imply that at low loads (< 2 pN), the motors are coupled loosely and not synchronized. At intermediate loads ($2 - 4$ pN), the motors become phase-locked. At higher loads (> 4 pN), where higher efficiency is needed, the load increases the coupling between motors and causes them to synchronize. This result may have implications to how the motors respond when transporting cargoes that encounter obstacles such as the cytoskeleton or other vesicles.

The phase portrait shown in Fig. 5.9 was constructed by coupling two identical motors through various loads. The load acts much like the cargo linker stiffness by increasing the coupling strength between motors. The fixed point becomes more sta-

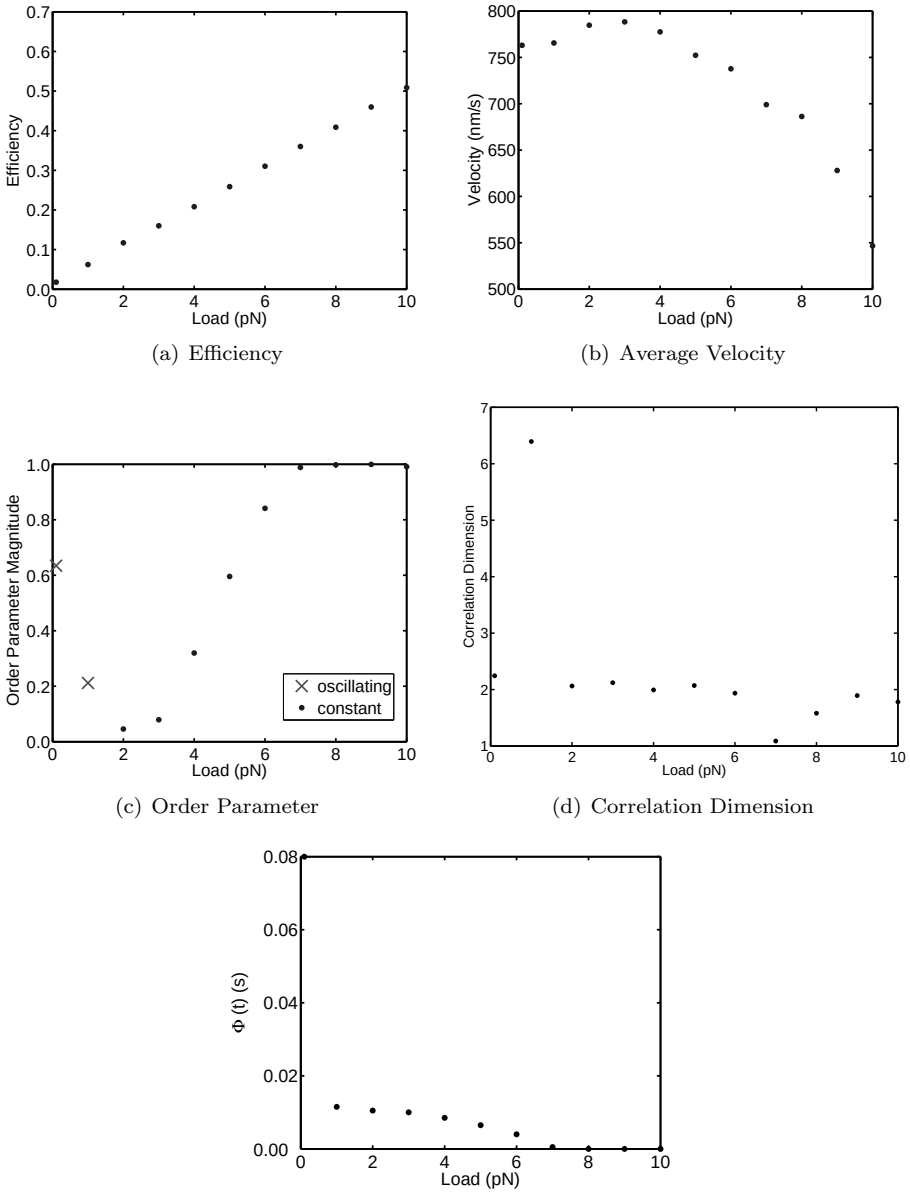

(a) Efficiency

(b) Average Velocity

(c) Order Parameter

(d) Correlation Dimension

(e) Phase Difference

Figure 5.10: The effect of the load on the synchronization. The difference in instrinsic velocity and cargo linker stiffness were constant, (std(k_{1f}) = 6 μMs^{-1}, $K_b = 0.5$ pN/nm).

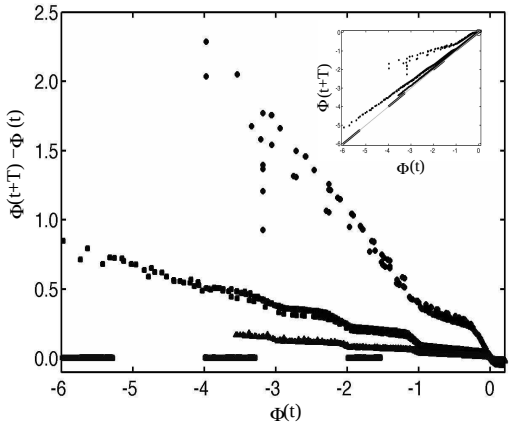

Figure 5.11: The effect of the load on the phase portrait of the phase difference for two identical coupled motors: Load = (■) 0 pN, (▲) 2 pN, (■) 4 pN, (●) 8 pN.

ble as the load is increased. At low loads, the speed at which the motors synchronize is low such that the motors would not synchronize in a typical run length of several hundred steps. At high loads, the motors synchronize quickly.

5.2.3 Effects of the Difference in Intrinsic Velocity

The dynamics of coupled motors are also affected by the degree of differences in the intrinsic velocity of the motors, as shown in Fig. 5.12. The chemical kinetics of the motors were varied through the parameter k_{1f}. This results in one of the motors hydrolyzing ATP faster than the other motor, leading to a difference in their intrinsic velocities. The cargo linker stiffness, K_b, and load were kept constant at 0.5 pN/nm and 2 pN, respectively. The efficiency did not change appreciably by varying the difference in intrinsic velocity. There is a local maximum of efficiency around a standard deviation of k_{1f} of 5 μMs^{-1}. This is surprising as one would expect the efficiency to decrease with the difference in intrinsic velocity. The velocity also exhibits a local maximum around std$(k_{1f}) = 5$ μMs^{-1}. The degree of synchronization provides an explanation for the increase in efficiency and velocity at std$(k_{1f}) =$ 5 μMs^{-1}. Similar to the variation in K_b, the motors are in a near-synchronous

dynamics when std(k_{1f}) is near 5μMs^{-1}, also corresponding to a local maximum in efficiency. The phase difference shows a tendency of the motors to lock onto a phase difference of 0.010 s around std(k_{1f}) = 5 μMs^{-1}, which is approximately one half of the period of the limit cycle, or a dynamics where head 1 of one motor is synchronized with head 2 of the other motor.

Several key observations on the synchronization of coupled kinesin motors can be made based on the parametric study. First, a higher degree of synchronization corresponds to greater efficiency and velocity, as demonstrated by local maxima in efficiency due to phase-locked states. Second, the relationship between coupling strength and degree of synchronization and between difference in intrinsic velocity and synchronization is not monotonic, i.e. greater coupling strength or uniformity does not directly correspond to a greater degree of synchronization. Third, increased loads lead to an increased degree of synchronization. At low loads (less than 2 pN), the motors are loosely coupled. At higher loads, the motors synchronize, resulting in greater efficiencies. This may be a mechanism for the motors to produce extra power to overcome obstacles in cells.

5.3 Discussion and Conclusions

To study the collective dynamics of kinesin-1, metrics to quantify the degree of synchronization were tailored to coupled nonlinear, nonsmooth oscillators. One such metric, the order parameter, provides a measurement of synchronization at the time scale of the motor limit cycle. However, the interpretation of the order parameter can be complicated by the period-2 limit cycle of kinesin-1, as well as oscillations in the order parameter at steady-state. The correlation dimension was used as another measurement of synchronization. Although the interpretation of the

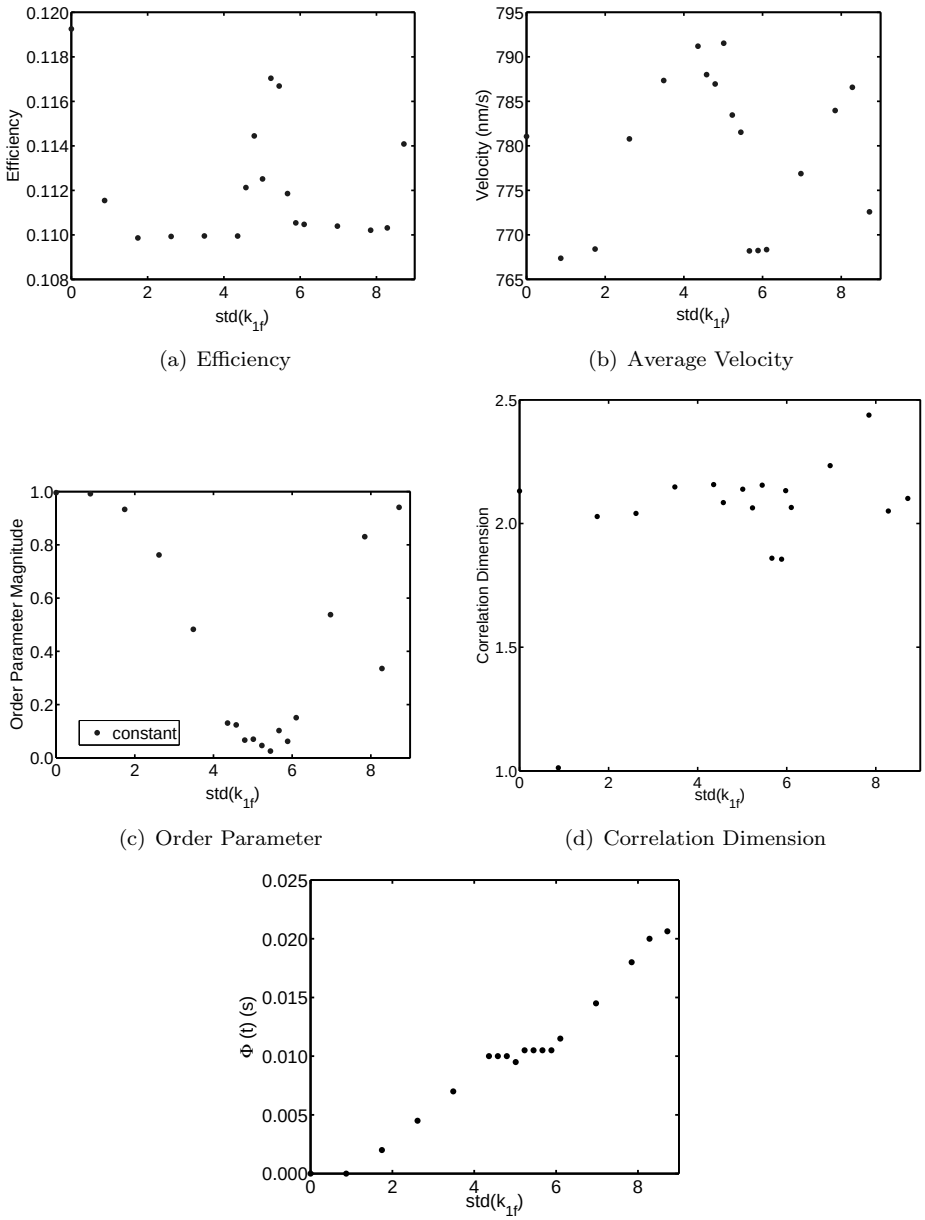

(a) Efficiency

(b) Average Velocity

(c) Order Parameter

(d) Correlation Dimension

(e) Phase Difference

Figure 5.12: The effect of the difference in intrinsic velocity std(k_{1f}) on the synchronization. The load and cargo linker stiffness were constant (Load = 2 pN, $K_b = 0.5$ pN/nm).

correlation dimension more intuitive, its calculation is more difficult. Also, since long time series are needed to calculate the correlation dimension, it does not provide an instantaneous measurement. The phase difference is a measurement of the absolute lag between motors in time. However, the interpretation of the phase difference may become difficult when large numbers of coupled motors are considered.

In a parametric study of two coupled kinesin motors, the metrics of synchronization were used to analyze the results of the mechanistic model. The effect of mechanical characteristics and load on the collective dynamics of kinesin-1 were investigated. There is a clear correlation between synchronization and efficiency, as a greater degree of synchronization leads to higher efficiency and higher velocity. This is evidenced in Figs. 5.8 and 5.12 where high degrees of synchronization correspond to local maxima in efficiency and velocity.

The experiments of Diehl et al. (2006) suggest that higher stiffness in the connection between motors leads to higher velocities in gliding assays. The results of our model agree, as Fig. 5.8 shows that, overall, increasing the cargo linker stiffness increases velocity and efficiency.

The model also suggests that at low loads, the motors are loosely-coupled and do not synchronize. However, higher loads increase the coupling strength and the motors synchronize, increasing their efficiency and thus the maximum force exerted. Motor proteins may operate similarly in the cell. The motors are usually under low load when transporting cargos and thus desynchronized. When the cargo encounters an obstacle such as the cytoskeleton or collisions with other vesicles, the motors synchronize to exert greater forces and overcome the obstacle.

Several researchers have observed faster transport in vivo than the maximum velocities implied by single-molecule in vitro experiments (18, 66, 70, 76). The

model results show that increased synchronization leads to larger velocities. However, the maximum increase in velocity predicted by the model due to synchronization between two motors was 10%, while velocities of up to 10 times the single-molecule velocity have been reported in some in vivo experiments tracking vesicle movement (66). Our modeling work is not consistent with such observations. It should be noted that it is not entirely certain which motors transported the vesicles and in some studies the observed increases in velocities were observed infrequently and over short distances (20 nm) as expected from short-term diffusive events (66). Possibly, the stochastic dynamics of the motors must be considered to observe the dramatic increase in velocity, or larger numbers of motors are involved in the transport in vivo. Alternatively, the large velocities observed in vivo may also be due to unrelated mechanisms such as the involvement of motors other than kinesin-1 or short-term elastic relaxations.

CHAPTER VI

Collective Dynamics of Motors with Stochastic Chemical Kinetics

In Chapter V, a deterministic, mechanistic model of kinesin-1 was developed and used to study the collective behavior of kinesin motor proteins transporting a common cargo. While the deterministic model gives first-order approximations of the collective dynamics, the dynamics of kinesin-1 are intrinsically stochastic due to the effect of thermal energy on the diffusion of the motor domain between binding sites and the chemical kinetics. Randomness may have a significant effect on the collective behavior. For example, two identical deterministic oscillators with identical initial conditions will follow exactly the same trajectory. However, if the oscillators are stochastic, the random component of the oscillator dynamics will differ for the two oscillators, such that although the oscillators are identical, their trajectories will differ. Accordingly, while coupled deterministic oscillators can become perfectly phase-locked, stochastic oscillators must overcome random effects to phase-lock. It is more likely that stochastic oscillators will, instead of becoming perfectly phase-locked, exhibit fluctuations about a phase-locked state. In this chapter, we extend the deterministic model to describe stochastic chemical kinetics, where the time-varying distributions of the chemical dwell time are taken into account. The mechanistic approach presented herein permits an efficient description of the stochastic, collective

dynamics of kinesin. We examine the effect of stochasticity on the collective behavior with respect to load, cargo linker stiffness, and the number of motors. The load and cargo linker stiffness are expected to have an effect on the collective behavior, as these parameters modulate the coupling strength between the motors, or the energetic incentive motors gain by synchronizing. Various numbers of motors are examined as intracellular transport is thought to involve teams of 2-10 motors (37, 39, 100).

6.1 Stochastic Chemical Kinetics

The model was extended to include stochastic chemical kinetics, whereby the time-varying effect of ATP concentration and internal stresses on the distribution of the chemical dwell time is taken into account. As the part of the dwell time associated with the diffusion of the motor domain between binding sites is much shorter than the part of the dwell time due to the chemical kinetics (see Fig. 2.5), only the effect of randomness on the chemical kinetics is considered. As in the deterministic model, each motor domain (head) is assumed to behave according to Michaelis-Menten kinetics, defined by one reversible reaction followed by an irreversible reaction. The rates are defined as

$$k_{1f} = k_{1f,0}, \tag{6.1}$$

$$k_{1b} = k_{1b,0} \exp\left[\frac{\frac{1}{2}\kappa\left|\psi_s - \Psi_c\right|^{n_c}}{k_B T}\right], \tag{6.2}$$

$$k_{2f} = k_{2f,0}, \tag{6.3}$$

where $k_{1f,0}$, $k_{1b,0}$, $k_{2f,0}$, Ψ_c, n_c, and κ are parameters in the model. We assume that there is an optimal molecule configuration for the chemical reaction to proceed, defined by Ψ_c. A configuration away from this optimal configuration presents an energy barrier to the chemical reaction, which is modeled by increasing the effective

k_{1b}. From Kuo et al. (63), the probability distribution of the chemical dwell time is,

$$f(t) = \frac{k_{1f}k_{2f}[ATP]^*}{2A}\left[exp(A+B)t - exp(B-A)t\right], \tag{6.4}$$

where

$$A = \sqrt{(k_{1f}[ATP]^* + k_{1b} + k_{2f})^2/4 - k_{1f}k_{2f}[ATP]^*} \text{ and,} \tag{6.5}$$

$$B = -(k_{1f}[ATP]^* + k_{1b} + k_{2f})/2. \tag{6.6}$$

The asterisk denotes that [ATP] is measured in μM. The probability distribution is then integrated to get the cumulative probability distribution,

$$\begin{aligned} c(t) = \frac{k_{1f}k_{2f}[ATP]^*}{2A}\Bigg[&\frac{1}{(A+B)}exp(A+B)t \\ &-\frac{1}{(B-A)}exp(B-A)t - \frac{1}{(A+B)} + \frac{1}{(B-A)}\Bigg], \end{aligned} \tag{6.7}$$

which varies from 0 to 1. A uniformly-distributed random variable, w, is sampled once for each step of the motor. The probability distribution of the chemical dwell time is computed at each time step in the simulation. The chemical dwell time corresponding to the value of the cumulative probability equal to the random variable for that step is taken as the instantaneous chemical dwell time T_C such that

$$c(T_C) = w_j, \tag{6.8}$$

where j is the step index. Typical distributions of the chemical dwell time are shown in Fig. 6.1. Increasing the forward rates (k_{1f} and k_{2f}) shifts the distributions to shorter chemical dwell times, while increasing the backward rate (k_{1b}) shifts the distributions toward longer chemical dwell times.

The heads are assumed to be in opposite structural states, so one variable is required to describe the structural state of both heads. The switching of structural

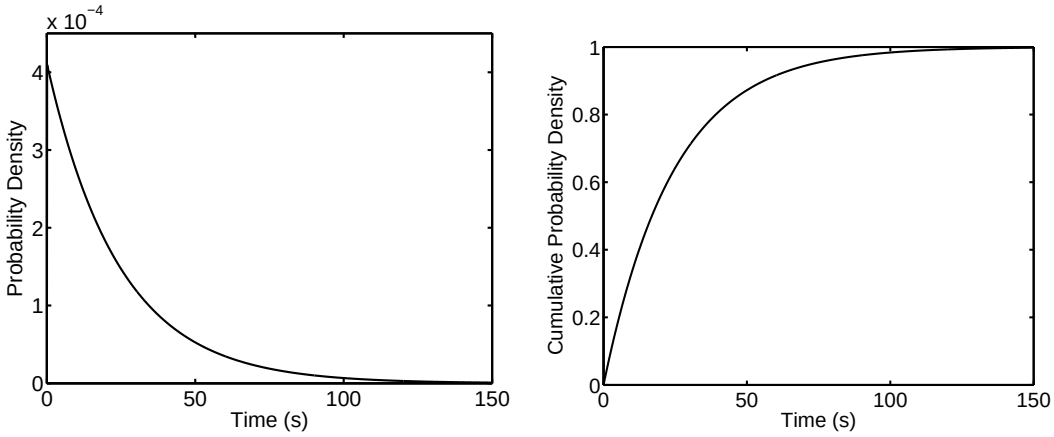

(a) (b)

Figure 6.1: The probability distributions of the chemical dwell time. For each step of the motor, a uniformly-distributed random variable is sampled, and used as the value of the cumulative probability for that cycle. While the random variable is constant for each cycle, the distributions are updated at each time step.

states (corresponding to the chemical or nucleotide states) is assumed to be dependent on the configuration of the motor and also on the ATP concentration. While one head is diffusing, the chemical state variable is approximately constant. Once the diffusing head is within 1% of the distance to the binding site, the rate of change of the chemical state variable is given by

$$\dot{\rho} = \pm \frac{[E]_t}{T_C} \tag{6.9}$$

where the total enzyme concentration $[E]_t$ is taken as $5 \cdot 10^3$ μM. To our knowledge, there is no available data for establishing the accuracy of the estimate of 1% of the distance between binding sites (0.08 nm). However, the overall results are only very weakly dependent on this parameter of the model. The chemical state variable, ρ, is considered to grow or decay until it reaches $\pm$ 1, at which time the structural state of both heads switch simultaneously.

The values of the parameters used in the model are unchanged from the values used in the deterministic model, summarized in Tab. 2.1. For the results in this

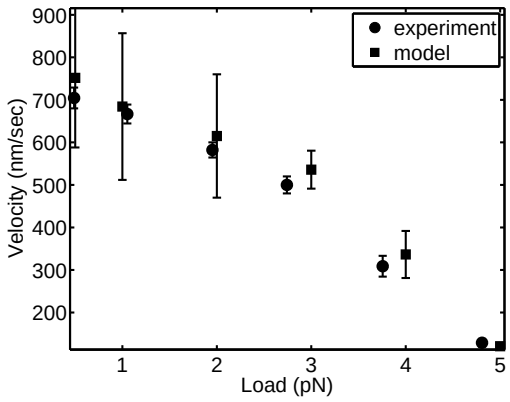

Figure 6.2: The stochastic model, using the same values of the parameters as the deterministic model, fits the experimental data from Block et al. (11) well.

chapter, the parameters corresponding to fit (a) for the single-molecule force-velocity data of Block et al. (11) are used. As shown in Fig. 6.2, the stochastic model fits the force-velocity data well.

6.2 Collective Motor Dynamics

The mechanistic model is able to describe the transient, stochastic dynamics of kinesin, making it well-suited to study the collective behavior of multiple motors transporting a common cargo. A typical realization of the deterministic model and the stochastic model for two coupled motors is compared in Fig. 6.3. The addition of stochastic chemical kinetics affects the collective dynamics. In the deterministic model, each motor exhibits a distinct dwell time, whereas the dwell time for the stochastic model is distributed. In Chapter V, metrics were developed to characterize the collective dynamics of nonlinear, nonsmooth oscillators such as kinesin. In this chapter, these metrics are used to investigate the effect of stochasticity on the collective dynamics of coupled kinesin motors, with respect to the cargo linker stiffness, load, and the number of motors. For each case, the data consists of 10 independent simulations of 50 steps.

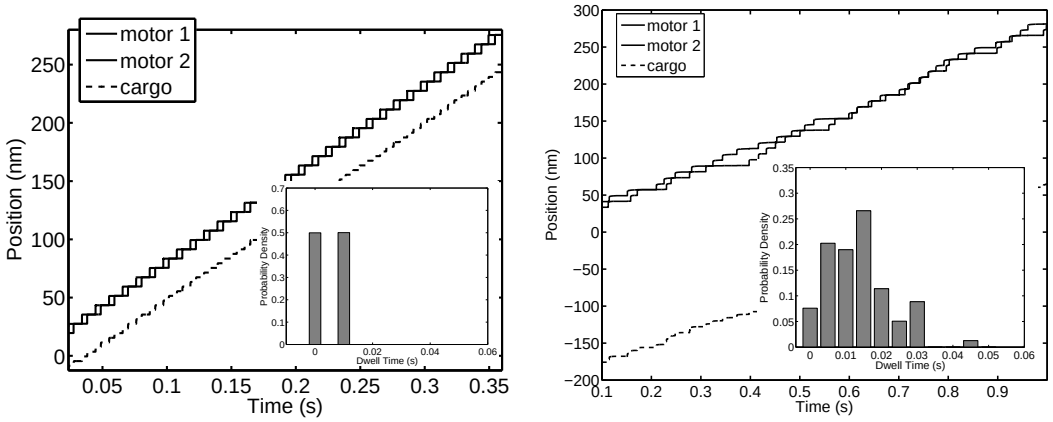

(a) Deterministic Model (b) Stochastic Model

Figure 6.3: Two coupled motors transporting a common cargo. The neck locations of the motors and the cargo location are shown. The deterministic motor exhibits one dwell time for each motor, while the stochastic model exhibits a distribution of dwell times.

6.2.1 Effect of Cargo Linker Stiffness

The stiffness of the cargo linker directly affects the coupling strength, or the energetic advantage the motors gain by synchronizing. As the stiffness increases, a difference in the strain of the cargo linkers of coupled motors translates to a larger difference in the load each motor carries. For example, if the cargo linker stiffness is 0.1 pN/nm and the difference in strain of the cargo linkers is 1 nm, the difference in load of the two motors is 0.1 pN. If the stiffness is increased to 1 pN/nm, the difference in the load becomes 1 pN. Thus, it is expected that the motors will tend to synchronize as the cargo linker stiffness is increased. The results of the model are consistent with this expectation, as is shown in Fig. 6.4. The fraction of energy in the phase-locked mode increases as the stiffness increases. The effect is more pronounced at higher loads, as higher loads increase the incentive to synchronize. The correlation dimension also increases with cargo linker stiffness, indicating that while the motors become more synchronized, the trajectory becomes more complicated. The standard deviation of the correlation dimension, shown by the error bars, also increases with

the cargo linker stiffness, indicating that stochasticity affects the trajectories more at higher cargo linker stiffness. In summary, the dynamics of the motors become more correlated with increasing load, while the trajectory of the motors becomes more complex temporally. Step size distributions were calculated using the cumulated step size data from all runs, and using a bin size of 0.5 nm. The value of the probability density of the step size distributions at the expected step size Δx_0 is shown in Fig. 6.4. The expected step size is taken as $\Delta x_0 = (8\text{ nm})/(\text{number of motors})$. For example, the step size of transport with a single kinesin motor is 8 nm. If two motors are transporting a cargo, and the motors are not stepping in synchrony, then the step size of the cargo will be 4 nm. The value of the probability density of the step size distributions at Δx_0 increases as the motors become more synchronized, indicating that the distribution narrows. At the highest stiffness, the probability density at Δx_0 decreases as the distribution broadens. This suggests that complexity in the trajectory, indicated by increases in the correlation dimension, causes the step size distribution to broaden while correlation between the motors, indicated by increases in the fraction of the energy in the phase-locked mode, causes the step size distribution to narrow.

6.2.2 Effect of Load

Like the effect of the cargo linker stiffness, the load also increases the coupling strength. The slope of the force-velocity curve increases from approximately 50 nm/s/pN for loads below 2 pN to approximately 200 nm/s/pN at loads greater than 3 pN. Therefore, for a given difference in the loads between motors, the difference in the average velocity of the two motors will increase with the load on the cargo. As shown in Fig. 6.5, the load increases the coupling strength, which in turn increases the amount of energy in the phase-locked mode. Analogous to the effect of increasing

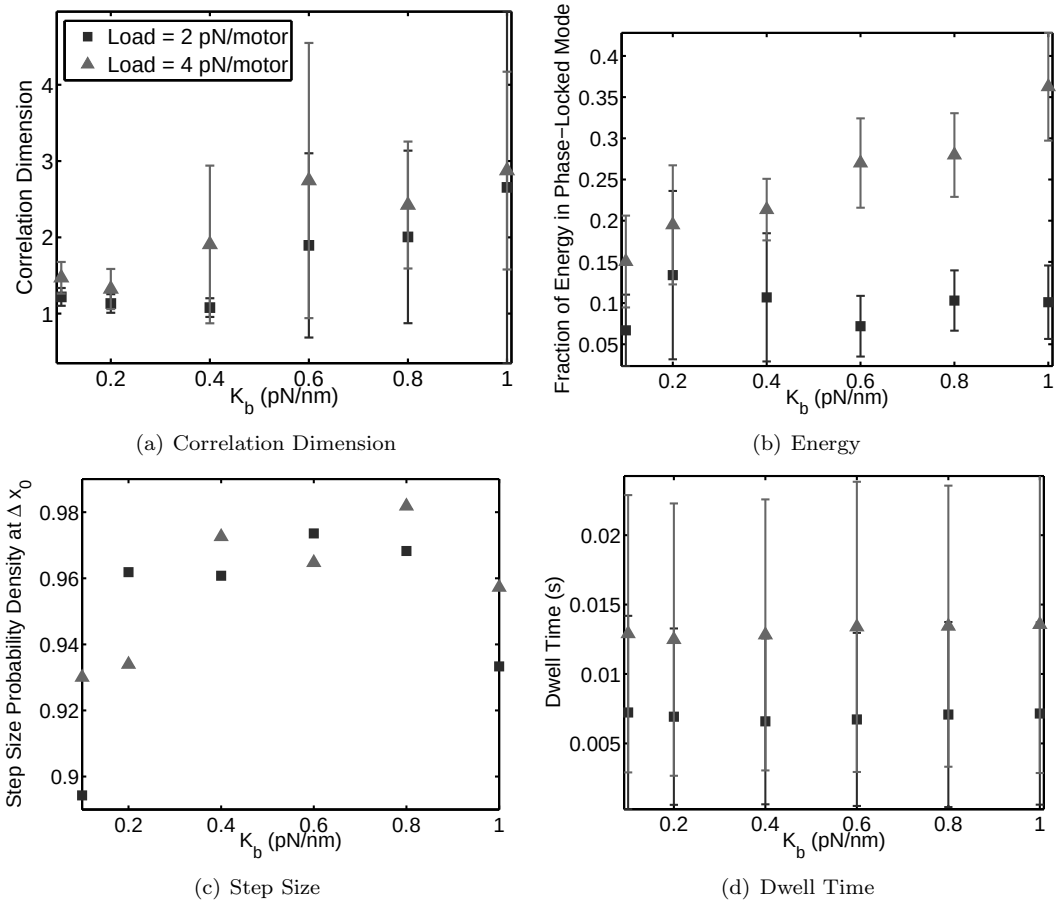

(a) Correlation Dimension

(b) Energy

(c) Step Size

(d) Dwell Time

Figure 6.4: The effect of cargo linker stiffness, K_b, on the collective dynamics of two kinesin motors transporting a common cargo. Legend: (■) Load = 2 pN/motor, (▲) Load = 4 pN/motor.

the coupling strength through the cargo linker stiffness, the correlation dimension also increases with load, indicating trajectories are more complex temporally at high loads. Load also increases the effect of stochasticity on the dynamics, as the standard deviation of the fraction of energy in the phase-locked mode and the correlation dimension increases with load. The results suggest that even for many coupled motors, the velocity is strongly correlated with the load per motor. The step size distribution narrows as the load is increased, evidenced by the value of the probability density at Δx_0 increasing with load.

6.2.3 Effect of Number of Motors

While the coupling strength is proportional to cargo linker stiffness and load, the number of motors does not effect the coupling strength. However, the chemical kinetics of each motor is dependent on random processes that are independent for each motor. Thus, each motor represents the addition of an independent random process to the system, suggesting that the degree of synchronization should decrease with the number of motors. As shown in Fig. 6.6, the fraction of energy in the phase-locked mode decreases with the number of motors. Alternatively, one may argue that because the velocity of the cargo becomes more constant as the number of motors increases, the forces on the motors must also become more constant, implying greater synchronization. However, while it is true that the total force on the cargo (i.e. the sum of the forces on all of the motors) becomes more constant with greater numbers of motors, the variance of the forces on each individual motor need not decrease. Consider the force $F = f_1 + f_2$. There are many cases where f_1 and f_2 can vary in time, but sum such that F is constant. Although the fraction of energy in the phase-locked mode decreases with the number of motors, the correlation dimension is not appreciably affected by the number of motors (the variation is within the

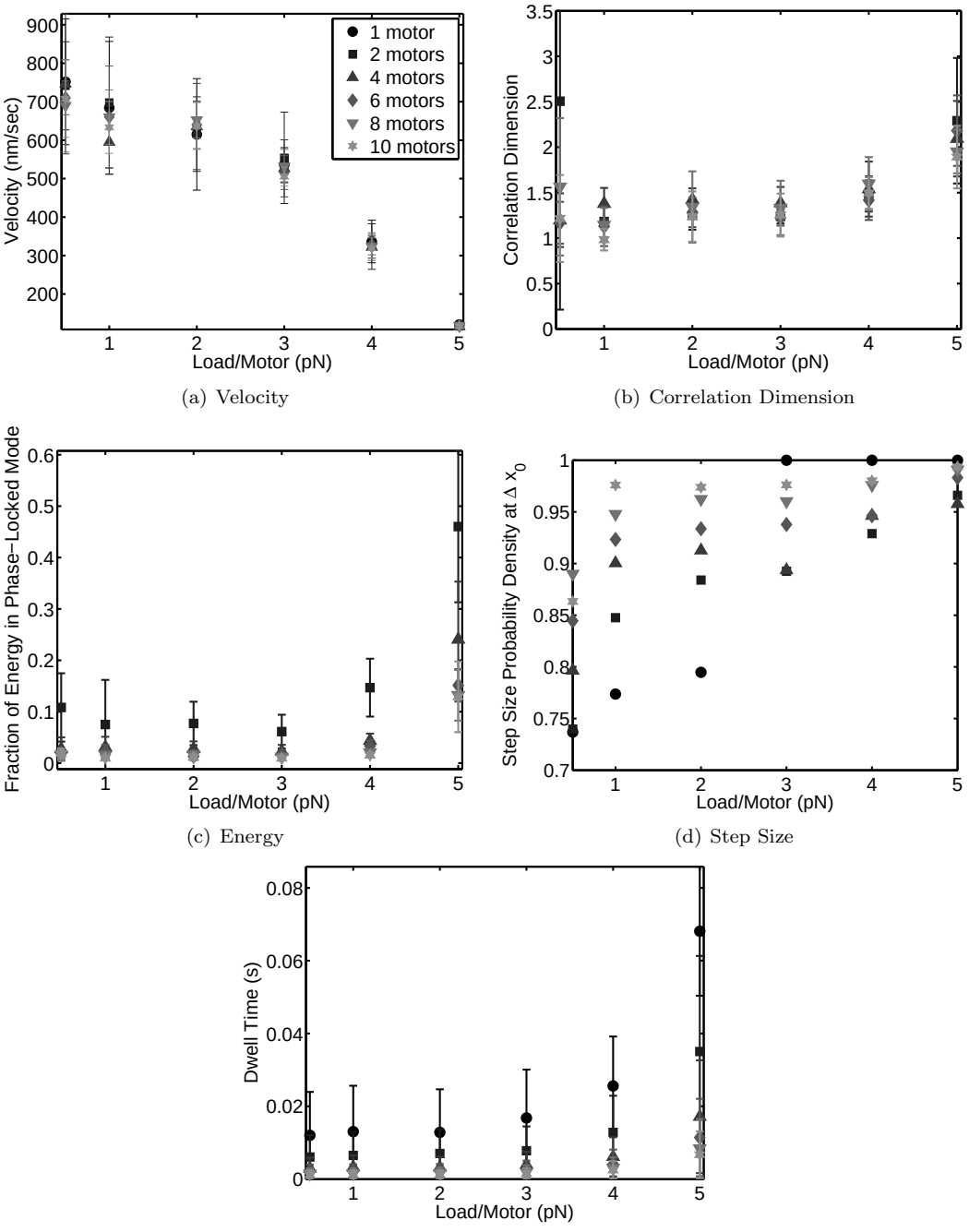

(a) Velocity

(b) Correlation Dimension

(c) Energy

(d) Step Size

(e) Dwell Time

Figure 6.5: The effect of the load on the collective dynamics of several kinesin motors, with cargo linker stiffness $K_b = 0.1$ pN/nm, transporting a common cargo. Legend: (•) 1 motor, (■) 2 motors, (▲) 4 motors, (♦) 6 motors, (▼) 8 motors, (∗) 10 motors.

standard deviation), indicating that the trajectory remains similar as the number of motors is increased. The value of the correlation dimension of approximately 1.5 indicates that the trajectory, in certain coordinates, lies on a torus. Taken together, the correlation dimension and energy analysis indicate that the dynamics of coupled motors are correlated. However, the correlation cannot be described by a constant phase between each motor. The step size distribution narrows with the number of motors, indicating that the step size distribution narrows as the correlation dimension decreases, as in Fig. 6.4. The mean step size decreases with the number of motors, indicating the motors are not fully-synchronized (phase-locked with a phase difference of 0), in agreement with the correlation dimension and energy analysis.

6.3 Discussion and Conclusions

In this chapter, the deterministic model was extended to include stochastic chemical kinetics, yielding a stochastic model capable of describing the transient dynamics of kinesin, making it well-suited to investigate the collective behavior of kinesin. While coupled deterministic motors are able to phase-lock at certain conditions, stochastic motors fluctuate about a phase-locked state. The coupling drives the motors to a phase-locked state, while stochastic fluctuations perturb the motors away from the phase-locked state. Despite this fundamental difference between deterministic and stochastic motors, the general conclusions drawn from the results of the deterministic model were validated by the stochastic model. The degree of synchronization increases when the coupling strength is increased, either through the cargo linker stiffness or the load. The model suggests that at low loads, the motors are loosely-coupled and do not synchronize. However, higher loads increase the coupling strength and the degree of synchronization increases, augmenting the efficiency and

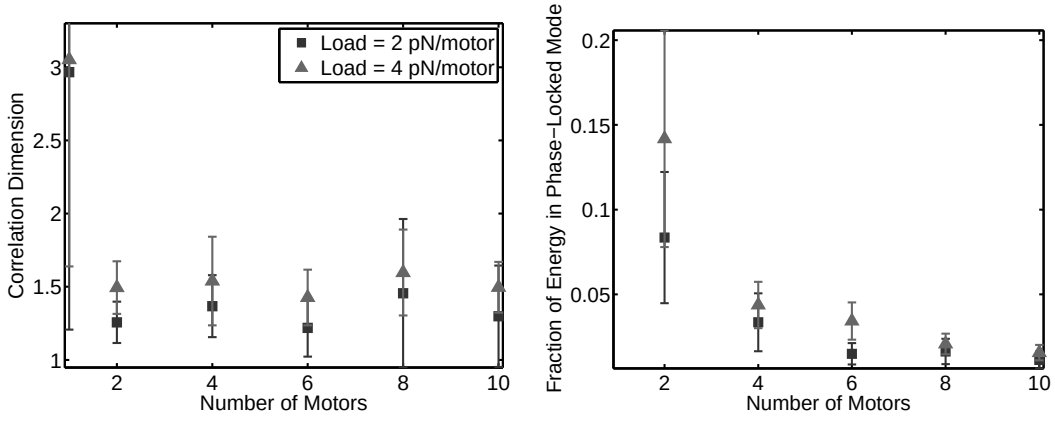

(a) Correlation Dimension

(b) Energy

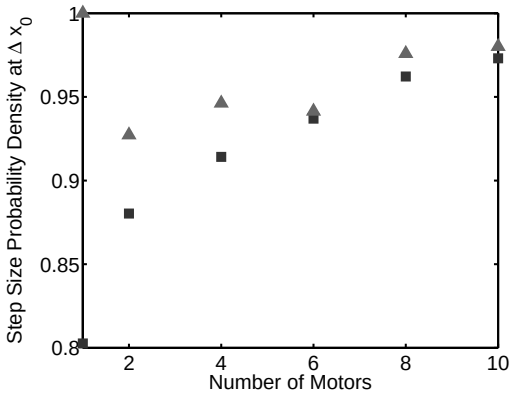

(c) Step Size

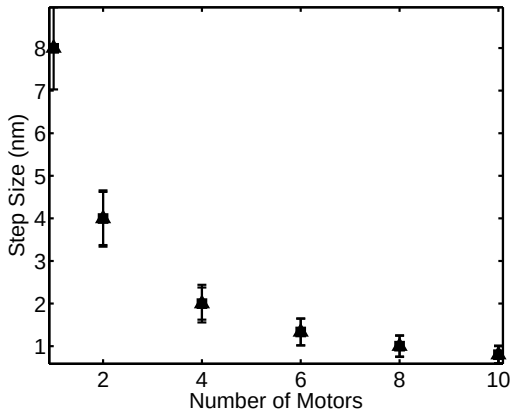

(d) Step Size

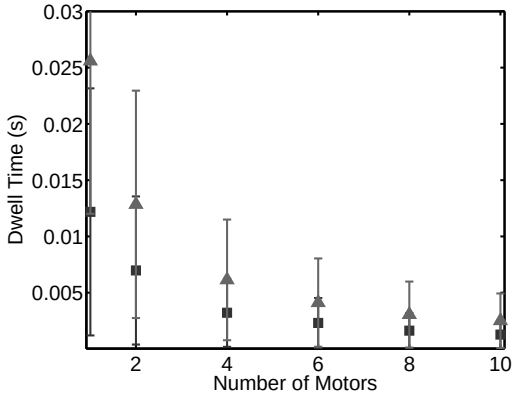

(e) Dwell Time

Figure 6.6: The effect of the number of motors on the collective dynamics of kinesin (K_b = 0.1 pN/nm). Legend: (■) Load = 2 pN/motor, (▲) Load = 4 pN/motor.

the maximum force exerted. This result may hold corollaries for transport in the cell, where for normal transport motor proteins are under low load and loosely correlated. When the cargo encounters an obstacle such as the cytoskeleton or collisions with other vesicles, the increased load causes the motors to become better correlated to allow them to overcome the obstacle.

The results of the model indicate that the degree of synchronization decreases with the number of motors, as evidenced by the fraction of energy in the phase-locked mode decreasing with the number of motors. At the same time, the dimensionality of the trajectory does not appreciably increase with the number of motors, suggesting that several motors interact such that their motion is highly correlated, but cannot be described by a constant phase difference between motors.

Several researchers have made in vivo observations of transport directed towards the plus end of the microtubule at velocities faster than the maximum velocities of kinesin implied by single-molecule in vitro experiments (18, 66, 70, 76). Velocities of up to 10 times the single-molecule velocity have been reported in some in vivo experiments tracking vesicle movement (66), suggesting that greater velocities may be due to the coordination of many kinesin motors. Our modeling work is not consistent with such observations. The results of the stochastic model predict that the force-velocity curve for coupled motors is very similar to the single-molecule force-velocity curve, when the velocity is plotted against the average load per motor, as shown in Fig. 6.5. Several explanations may account for this discrepancy. For example, in the in vivo experiments it is not certain which motors transported the vesicles. Also, in some studies, the observed increases in velocities were observed infrequently and over short distances (20 nm) as expected from short-term diffusive events (66). Possibly, the fundamental head-to-head coupling of kinesin changes when in a multiple-motor

orientation, and must be considered to observe the dramatic increase in velocity, or larger numbers of motors (greater than 10) are involved in the transport in vivo. Alternatively, the large velocities observed in vivo may also be due to unrelated mechanisms such as the involvement of motors other than kinesin-1 or short-term elastic relaxations.

CHAPTER VII

Discussion and Conclusions

Herein, a mechanistic approach was used to develop a dynamic, mathematical model for the collective behavior of kinesin. The mechanistic model accounts for previously published results of the mechanical behavior of single kinesin molecules, and is also capable of predicting the cooperative interactions of multiple kinesin molecules. In particular, the model accounts for the unsteady interactions between the mechanochemical cycle of each motor to the other coupled motors. This is distinct from multi-state kinetic and thermal ratchet approaches, which are focused on single molecules carrying a constant load, under the assumption of quasi-equilibrium that requires that the loads carried by each molecule or motor domain alone be constant (3, 4, 28–30, 53, 95, 96, 107).

Based on the existing knowledge of structure-function relation of kinesin, the governing equation for the mechanical characteristics, stress conditions, and the chemical kinetics of a motor domain have been modeled. The models for these domains were then used as building blocks to obtain a full model of the motor by accounting for the mechanical coupling between domains. Particular emphasis has been placed on the mechanistic aspects of the motor protein. Specifically, the full model accounts for the distribution of forces (stresses) throughout all domains of the motor. The mechanis-

tic perspective of the model is reinforced by an explicit description of the coupling mechanism between the chemical and the mechanical dynamics. The stresses in each domain are used to account for changes in their chemical kinetics. Both the mechanical and the chemical dynamics are characterized for the fully unsteady response of each domain (i.e. the response caused by time and space varying external loads, stresses between domains, and stresses between motors). Such a detailed temporal and spatial modeling approach leads to severe complexities if one attempts to model directly the stochastic nature of the process, such as through Monte Carlo simulations. Monte Carlo simulations are computationally expensive, and provide limited insights when multiple motors and their phase-locked dynamics are of interest. Herein, an alternate approach has been demonstrated. A mechanistic model has been constructed by modeling the (statistical) average dynamics of each domain through a set of deterministic governing equations. The deterministic approach has been shown to predict the mean behavior through Monte Carlo simulations. The deterministic model was then extended to describe the effect of stochastic chemical kinetics, through a novel and efficient description of the time-varying distributions of the chemical dwell time. Finally, the mathematical representations of the mechanics (stresses) and chemistry (chemical kinetics) of each domain were combined to obtain the full model for one motor or for a number of coupled motors. The bottom-up approach used in constructing this model ensures that *all* mechanistic couplings are taken into account, allowing the mechanistic model to predict both steady-state and transient dynamics.

In contrast to previous models of kinesin movement, the mechanistic model was developed that predicts steady state and transient dynamics through use of a simplified mechanical energy storage and mean first-passage time. Alternating hydrolysis

in the two motor domains was accounted for through modeling the dependence of the chemical kinetics of each head on the configuration of the molecule. The model indicates that the internal stresses assist diffusion for approximately half of each step, and opposes diffusion for the remainder of each step, possibly explaining the observation of sub-steps in the kinesin cycle. The stresses in the molecule then bias the chemical kinetics such that the rear head becomes weakly-bound and the forward head becomes strongly-bound, allowing the cycle to repeat. The model also provides a means of explaining the changes in the shape of the force-velocity curve with ATP concentration through the diffusion ratio. The chemical kinetics are highly ATP dependent, while diffusion is not. Thus, the diffusion ratio, or ratio of time spent diffusing to the time waiting for the chemical reaction to proceed, must be ATP dependent. The dependence of the diffusion ratio on ATP concentration mirrors the changes in the shape of the force-velocity curve.

Importantly, the model proposed herein is able to account for the transient dynamic response of each domain (or each motor, when multiple motors are studied). This feature allows for establishing the stability characteristics of the synchronous or phase-locked motion of multiple coupled motor domains or multiple coupled motors. Recently, aspects of the coupling between motor domains have been investigated through a biosynthetic approach (24). The cooperativity between motor domains of kinesin has been observed to enhance hydrolysis activity, while the resulting transport was observed to be distinct from that caused by cooperativity of multiple motor proteins carrying a common load. Hence, the mechanical coupling between motor domains, and that between multiple motors plays a critical influence on force-velocity characteristics. To model this coupling, it is crucial that the force exerted by each motor domain be characterized *during* each mechanochemical cycle because synchro-

nization and phase locking are sustained by coupling effects of the motion of one motor domain (or molecule) with the others *during* each mechanochemical cycle, i.e. the timescale of the forces is faster than the timescale of the mechanochemical cycle.

Current models of motor proteins are not well suited to describing transient motion. In existing kinetic models, the dynamics are only defined at a small number of discrete spatial locations (1 to 4 per step). Thus, the coupling between separate molecules or motor domains cannot be resolved accurately because this coupling is dependent on the location of each motor (domain) in the ensemble. Also, the rates between states are assumed to be constant in current models, in effect assuming constant potentials. Thus, current kinetic models of kinesin are able to model transients due to the initial probability distribution, but not due to perturbations during the motion. Similarly, thermal ratchet models assume constant potentials which do not change in response to unsteady forces during the motion. The Fokker-Planck equation is then solved for stationary solutions, i.e. the time derivatives are set to zero. Consequently, by assuming constant transition rates and potentials, current kinetic models and thermal ratchet models of kinesin are unable to predict transient motion due to unsteady loads.

The mechanistic approach herein yields a simple model with certain limitations. Stochastic behavior is only partially characterized. For example, the model cannot, in its current form, describe mean run length (processivity) data. Another consequence is that although the first-passage time calculation considers forward and reverse transitions during diffusion, once the diffusing head reaches the binding site, it is considered to bind irreversibly. Hence, backward steps are not modeled, although backward steps have been observed to occur occasionally in experiments. In addition, the simplified geometric configuration of the model limits its ability to

explain the experimental data which predicts that sideways loads accelerate kinesin movement (11). It is likely that the internal stresses contain a twist component, which would explain acceleration in response to sideways forces. Nonetheless, the twisting component can be quite easily incorporated in the mechanistic modeling approach herein, whereas accounting for such twisting in other current kinetic or ratchet models is not as straightforward.

Despite the limitations above, the mechanistic approach has many advantages over existing models. First, the mechanistic formulation of this model provides a description of the transient dynamics, in addition to describing steady-state dynamics. Knowledge of the transients allows investigation of unsteady loads and the cooperative dynamics resulting from interaction among many motors. Existing stochastic models are restricted to describe the steady-state motion of the motor protein. Second, in the mechanistic model, no assumption was made *a priori* on the relative importance of diffusion, relaxation, and ATP hydrolysis on the dynamics of the motor. Instead, the relative importance of these quantities becomes evident from experimental data used to identify these parameters. The coupling of the mechanics to the chemical kinetics is described explicitly through the effect of the time-varying geometry of the molecule on the chemical rates.

The utility of the formulation herein is illustrated in the following example. Consider a single kinesin motor pulling a bead. The bead is released from rest. What is the resulting motion? A thermal ratchet model, restricted to a constant potential, could not account for non-constant forces. Thus, a thermal ratchet model would only be accurate for steady-state motion. Similarly, a kinetic model would be difficult to use. Such a model would predict an initial transient due to the initial probability distribution at $t = 0$. However, with constant transition rates, a kinetic model

could not consider time-varying loads. Thus, like thermal ratchet models, a kinetic model would only be accurate at long times, once the force on the motor is constant. The mechanistic model developed here, though, is able to accurately describe the time-varying load at each instant of the motion. Thus, the deterministic formulation would accurately predict the transient motion of the motor and bead, as well as the motion once the system reached steady state. Moreover, vesicles are known to collide with one another and the cytoskeleton in the cell. In this case, a thermal ratchet model fails, as the potential is constant, and cannot change in response to the collision. Similarly, a kinetic model would need to be significantly modified so as to include an alternate pathway, where the transition rates (e.g. load coefficients (29, 30) $\theta_{1,2,3,...}$) would be affected in response to the changed (increased) load.

One of the goals of the study, apart from developing a mechanistic model of kinesin, was to develop the tools necessary to characterize the the dynamics of nonlinear, nonsmooth coupled oscillators. Towards this goal, several metrics were tailored to quantify the collective dynamics of nonlinear, nonsmooth coupled oscillators. The complex order parameter had previously been used to analyze simple, one-degree-of-freedom oscillators (67). We extended its use to nonlinear, nonsmooth oscillators. In addition, the use of the correlation dimension as a measurement of synchronization was demonstrated. Lastly, a method to quantify the fraction of energy in the phase-locked mode of the oscillators was developed. These metrics provide the tools to characterize the collective dynamics of nonlinear, nonsmooth oscillators like kinesin.

The overarching goal of this study was to provide a link between the data on kinesin gained from single molecule experiments and the behavior of kinesin in cells, where it is likely that kinesin functions collectively in teams of several motors to drive intracellular transport. Specifically, the study aimed to answer several questions

central to cell biology: Do coupled kinesin motors synchronize, or function largely independently? How do large numbers of motors interact such that the speed is unaffected? What advantage does kinesin gain by working in teams? The mechanistic model and metrics of synchronization developed herein comprise the tools needed to make quantitative predictions of the collective dynamics of kinesin, providing a means to answer these questions.

The predictions made by the mechanistic model suggest that the degree of synchronization of coupled kinesin motors is dependent on the mechanical properties of the motors, the load, and the number of motors involved in the transport. While the motors never completely synchronize, the degree of synchronization increases when the coupling strength is increased, either through the cargo linker stiffness or the load. At low loads, the motors are loosely-coupled and do not synchronize. However, higher loads increase the coupling strength and cause the degree of synchronization to increase, augmenting the efficiency and the maximum force exerted. This result likely holds corollaries for transport in the cell, where motor proteins are usually under low load when transporting cargos and their dynamics are loosely correlated. When the cargo encounters an obstacle such as the cytoskeleton or collisions with other vesicles, the dynamics of the motors become better correlated in response to higher loads, allowing them to overcome the obstacle. The behavior of coupled motors in response to load also points to an advantage that kinesin gains by functioning collectively. Kinesin motors are coupled in such a way that they do not interfere with each other during normal transport. However, when they encounter an obstacle, they can become more synchronized to produce greater forces. Unfortunately, current experimental observations of intracellular transport do not provide a measurement of the load. Likewise, the cargo linker stiffness of kinesin has not been

measured accurately. Data from future experiments is therefore needed to refine the predictions of the model.

Current experiments estimate intracellular transport is driven by teams of 2-10 motors. The results of the model indicate that the degree of synchronization decreases with the number of motors, as evidenced by the decrease in the fraction of energy in the phase-locked mode with increasing numbers of motors. At the same time, the dimensionality of the trajectory does not appreciably increase with the number of motors, suggesting that several motors interact such that their motion is highly correlated, but cannot be described by a constant phase lag between motors. The correlation dimension suggests that although several coupled kinesin motors do not fully synchronize, their dynamics are highly correlated, allowing several motors to function collectively such that the speed of the transport is not degraded.

Several researchers have made in vivo observations of transport directed towards the plus end of the microtubule at velocities faster than the maximum velocities of kinesin implied by single-molecule in vitro experiments (18, 66, 70, 76). Velocities of up to 10 times the single-molecule velocity have been reported in some in vivo experiments tracking vesicle movement (66), suggesting that high velocities may be due to the coordination of many kinesin motors. Our modeling work is not consistent with such observations. The results of the stochastic model predict that the force-velocity curve for coupled motors is very similar to the single-molecule force-velocity curve, when the velocity is plotted against the average load per motor, as shown in Fig. 6.5. Several explanations may account for this descrepancy. For example, it is not certain which motors transported the vesicles. Also, the high velocities were observed infrequently and over short distances (20 nm) and thus may be due to short diffusive events (66). Possibly, the fundamental head-to-head coupling of

kinesin changes when in a multiple-motor orientation, and must be considered to observe the dramatic increase in velocity, or larger numbers of motors (greater than 10) are involved in intracellular transport. Alternatively, the large velocities observed in vivo may also be due to unrelated mechanisms such as the involvement of motors other than kinesin-1 or short-term elastic relaxations.

The model makes several quantitative predictions on the collective dynamics of kinesin that can now be compared to experiments. First, the model predicts that the force-velocity curve for multiple, coupled motors transporting a load closely matches the single-molecule force-velocity curve, when the velocity is plotted against the average load per motor. In addition, the relationship between the correlation dimension and cargo linker stiffness, load, and number of motors can be compared to force-clamp measurements of transport by multiple kinesin motors. The correlation dimension can be calculated from the record of the bead locations in time using embedded coordinates (92). Step size distributions and dwell time distributions can also be compared to experiment, using a step-finding algorithm such as the one used by Kerssemakers et al. (58). The model proposed herein assumes that the mechanisms of kinesin do not change fundamentally when functioning collectively, i.e. the mechanisms of each motor involved in coordinated transport are synonymous with the single-molecule operation, with the exception of time-varying loads induced on each motor through their interaction. Comparisons of the results of the model with experiment have the potential to elucidate a fundamental question of intracellular transport: Are the single-molecule mechanisms of kinesin, such as head-to-head coordination, analogous to the collective mechanisms of kinesin motors?

The understanding of bio-mechano-chemical processes as well as the development of emerging applications of these processes in lab-on-a-chip paradigms (45, 71, 103)

are importantly dependent on the ability to predict and model the cooperativity of motor proteins transporting a common cargo. The goal of the model demonstrated herein is to provide a link between single-molecule studies and the dynamics of groups of motor proteins, with a focus on kinesin. The dynamics of teams of motors can be dramatically distinct from one motor alone. For example, *in vivo* collective transport by several motors in living cells is expected to differ significantly from observed single-molecule transport by various measures (e.g. velocity, run length) (24, 37, 39, 66, 70, 76, 100). In particular, an array of instabilities and complex oscillatory dynamics may be experienced by groups of otherwise simple dynamical systems (91). In the case of motor proteins, such dynamics are due to cooperativity, and are likely the cause for oscillations observed in a number of biological systems. For example, dynamic instabilities in the actomyosin are thought to be responsible for the rapid dynamics in insect flight muscles (25). Also, the collective dynamics of teams of motors could explain the movement and dynamic properties of spermatozoid flagella (15) through cooperativity of axonemal dynein motors, and may be the cause for the high sensitivity of mechanical sensing (16) such as detecting sound in the cochlea (36, 50, 108) through cooperativity of prestin motors. Moreover, the increasing use of the complex dynamics of teams of motors in artificial engineered systems such as nano-scale molecular sorting devices (45, 103) requires models well suited for characterizing mechanochemical cooperativity and fundamental mechanical phenomena which govern collective molecular transport.

7.1 Future Research

The goal of this effort is to provide a mechanistic understanding of the link between single-molecule biophysics and cell biology. Single kinesin molecules have been well-

characterized through in vitro experiments. However, the understanding of single molecules has not lead to a complete understanding of kinesin behavior in cells, partially due to the significant differences between single-molecule dynamics and the collective dynamics of several coupled motors. The inability to link single-molecule biophysics to cell biology is common in motor proteins. For example, although the single-molecule behavior of dynein is characterized, the collective behavior in cilia and flagella is not well understood. The same is true for myosin in skeletal muscle. The approach described herein seeks to provide a novel, mechanistic framework to link knowledge from single-molecule studies to cell biology.

To meet this goal, we must develop an understanding of the collective dynamics of coupled kinesin motors. The first step, developing a mechanistic, transient model of single kinesin molecules, is complete. Metrics of synchronization, specifically tailored to nonsmooth, nonlinear oscillators like motor proteins, were developed. The results of the mechanistic model suggest that the trajectory of the dynamics of many coupled kinesin motors can be described by only a few coordinates. However, the fraction of energy in the phase-locked mode is small. To better characterize the correlation between coupled motors, the energy analysis should be extended to allow for the possibility of a time-varying, periodic phase between oscillators.

The mathematical description of kinesin-1 completed thus far should now be used as a platform for further studies into central questions about the mechanism of kinesin-1. One central question is the asymmetry observed in the velocity of kinesin-1 when subjected to sideways loads (11). By using current structural data to extend the current model to three dimensions, the increased velocities when kinesin is subjected to loads perpendicular to the direction of transport can be described.

Single-molecule studies of kinesin-1 suggest that a single motor has a run length of

approximately 1 μm before detaching from the microtubule. However, many neurons extend to lengths of several meters. Thus, in vivo, kinesin-1 must be capable of transporting cargos much greater distances than the run length of a single motor. By extending the model to include detachment from the microtubule, the effect of collective behavior on the run length can be investigated.

Due to the complex, multi-scale nature of transport in the cell; quantitative, mathematical models are essential for focusing experimental efforts. For instance, previous experiments suggest that the velocity of a microtubule being transported by kinesin motors is independent of the number of motors (48). These experiments were conducted at low loads, as no external force was applied to the microtubule. However, the results of the mechanistic model show that the effects of collective behavior are only apparent at moderate to high loads. Thus, we designed an experiment to observe the collective behavior of kinesin-1 when a force is applied to the microtubule. As in previous experiments, kinesin-1 motors were bound to the substrate. Microtubules interacted with the motor domains of the kinesin and were transported, with several motors being coupled through the microtubule and substrate. The concentration of kinesin in the assay is used to estimate the number of motors interacting with a microtubule. To examine collective transport under an applied load, a latex bead is bound to the microtubule through biotin-streptavidin linkages. Forces are then applied to the bead using an optical trap or a magnetic field.

Future experiments should characterize the mechanical properties of the cargo linker. Experiments should also be designed to test the effect of the cargo linker stiffness on the collective transport, possibly by expressing several constructs of kinesin-1. In each of these constructs, a flexible domain could be appended to the cargo linker, with the length of the flexible domain corresponding the the stiffness of the molecule.

The experiments should also be extended by including a measurement of the number of kinesin motors involved in the transport. For instance, a fraction of the ATP in solution could be labeled with a fluorophore. The Flourescence Resonance Energy Transfer (FRET) signal resulting from the interaction of fluorescently-labelled ATP molecule and the fluorescently-labeled microtubule could be observed. This experiment would represent the first observation of a gliding assay where the number of motor proteins interacting with the microtubule is measured.

Bibliography

[1] C L Asbury, A N Fehr, and S M Block. Kinesin moves by an asymmetric hand-over-hand mechanism. *Science*, 302:2130–2134, 2003.

[2] R D Astumian. Thermodynamics and kinetics of a Brownian motor. *Science*, 276:917–921, 1997.

[3] R D Astumian and I Derenyi. A chemically reversible Brownian motor: Application to kinesin and Ncd. *Biophysical Journal*, 77:993–1002, 1999.

[4] M Badoual, F Julicher, and J Prost. Bidirectional cooperative motion of molecular motors. *Proceedings of the National Academy of Science*, 99(10):6696–6701, 2002.

[5] H C Berg. *Random Walks in Biology*. Princeton University Press, Princeton, NJ, 1993.

[6] M Bier. The noisy steps of a motor protein. In American Institute of Physics, editor, *CP655, Unsolved Problems of Noise and Fluctuations: UPoN 2002: Third International Conference*, pages 290–297, 2003.

[7] M Bier. Modelling processive motor proteins: Moving on two legs in the microscopic realm. *Contemporary Physics*, 46(1):41–51, 2005.

[8] M Bier. The stepping motor protein as a feedback control ratchet. *Biosystems*, 88:301–307, 2007.

[9] M Bier. Brownian ratchets in physics and biology. *Contemporary Physics*, 38(6):371–379, 1997.

[10] S M Block, L S B Goldstein, and B J Schnapp. Bead movement by single kinesin molecules studied with optical tweezers. *Nature*, 348:348–352, 1990.

[11] S M Block, C L Asbury, J W Shaevitz, and M J Lang. Probing the kinesin reaction cycle with a 2D optical force clamp. *Proceedings of the National Academy of Science*, 100(5):2351–2356, 2003.

[12] G S Bloom, M C Wagner, K K Pfister, and S T Brady. Native structure and physical properties of bovine brain kinesin and identification of the ATP-binding subunit polypeptide. *Biochemistry Journal*, 27:3409–3416, 1988.

[13] S T Brady. A novel brain ATPase with properties expected for the fast axonal transport motor. *Nature*, 317:73–75, 1985.

[14] D Cai, K J Verhey, and E Meyhöfer. Tracking single kinesin molecules in the cytoplasm of mammalian cells. *Biophysical Journal*, 92:4137–4144, 2007.

[15] S Camalet, F Julicher, and J Prost. Self-organized beating and swimming of internally driven filaments. *Physical Review Letters*, 82(7):1590–1593, February 1999.

[16] S Camalet, T Duke, F Julicher, and J Prost. Auditory sensitivity provided by self-tuned critical oscillations of hair cells. *Proceedings of the National Academy of Sciences*, 97(7): 3183–3188, March 2000.

[17] N J Carter and R A Cross. Mechanics of the kinesin step. *Nature*, 435:308–312, 2005.

[18] S Courty, C Luccardini, Y Bellaiche, G Cappello, and M Dahan. Tracking individual kinesin motors in living cells using single quantum-dot imaging. *Nano Letters*, 6(7):1491–1495, 2006.

[19] J D Crawford and K T R Davies. Synchronization of globally coupled phase oscillators: Singularities and scaling for general couplings. *Physica D*, 125:1–46, 1999.

[20] R A Cross. Directing direction. *Nature*, 406:839–840, 2000.

[21] R A Cross. The kinetic mechanism of kinesin. *Trends in Biochemical Sciences*, 29(6):301–309, 2004.

[22] M de Cuevas, T Tao, and L S B Goldstein. Evidence that the stalk of Drosophila kinesin heavy chain is an alpha-helical coiled-coil. *Journal of Cell Biology*, 116:957–965, 1992.

[23] I Derenyi and T Vicsek. The kinesin walk: a dynamic model with elastically coupled heads. *Proceedings of the National Academy of Science*, 93:6775–6779, 1996.

[24] M R Diehl, K Zhang, H J Lee, and D A Tirrell. Engineering cooperativity in biomotor-protein assemblies. *Science*, 311:1468–1471, 2006.

[25] T Duke. Push or pull? Teams of motor proteins have it both ways. *Proceedings of the National Academy of Science*, 99(10):6521–6523, 2002.

[26] S A Endow. Determinants of molecular motor directionality. *Nature Cell Biology*, 1:E163–E167, 1999.

[27] B P English, W Min, A M van Oijen, K T Lee, G Luo, H Sun, B J Cherayil, S C Kou, and X S Xie. Ever-fluctuating single enzyme molecules: Michaelis-Menten equation revisited. *Nature Chemical Biology*, 2(2):87–94, February 2006.

[28] M E Fisher and Y C Kim. Kinesin crouches to sprint but resists pushing. *Proceedings of the National Academy of Sciences*, 102(45):16209–16214, 2005.

[29] M E Fisher and A B Kolomeisky. Simple mechanochemistry describes the dynamics of kinesin molecules. *Proceedings of the National Academy of Science*, 98(14):7748–7753, 2001.

[30] M E Fisher and A B Kolomeisky. Molecular motors and the forces they exert. *Physica A*, 274:241–266, 1999.

[31] R F Fox and M H Choi. Rectified Brownian motion and kinesin motion along microtubules. *Physical Review E*, 63:051901, 2001.

[32] S P Gilbert, M R Webb, M Brune, and K A Johnson. Pathway of processive ATP hydrolysis by kinesin. *Nature*, 373:671–676, 1995.

[33] S P Gilbert, M L Moyer, and K A Johnson. Alternating mechanism of the kinesin ATPase. *Biochemistry Journal*, 37:792–799, 1998.

[34] L S B Goldstein. Kinesin molecular motors: Transport pathways, receptors, and human disease. *Proceedings of the National Academy of Sciences*, 98(13):6999–7003, 2001.

[35] P Grassberger and I Procaccia. Measuring the strangeness of strange attractors. *Physica D*, 9:189–208, 1983.

[36] K Grosh, J F Zheng, Y Zou, E de Boer, and A L Nuttall. High-frequency electromotile responses in the cochlea. *Journal of the Acoustical Society of America*, 115(5):2178–2184, MAY 2004.

[37] S P Gross, M C Tuma, S W Deacon, A S Serpinskaya, A R Reilein, and V I Gelfand. Interactions and regulation of molecular motors in Xenopus melanophores. *The Journal of Cell Biology*, 156:855–865, 2002.

[38] J Guckenheimer and P Holmes. *Nonlinear Oscillations, Dynamical Systems, and Bifurcations of Vector Fields*, volume 42 of *Applied Mathematical Sciences*. Springer-Verlag, 1983.

[39] S Gunawardena and L S B Goldstein. Cargo-carrying motor vehicles on the neuronal highway: Transport pathways and neurodegenerative disease. *Journal of Neurobiology*, 58:258–271, 2004.

[40] D D Hackney. Highly processive microtubule-stimulated ATP hydrolysis by dimeric kinesin head domains. *Nature*, 377:448–450, 1995.

[41] D D Hackney. The kinetic cycles of myosin, kinesin, and dynein. *Annual Review of Physiology*, 58:731–750, 1996.

[42] D D Hackney and M F Stock. Kinesin's IAK tail domain inhibits initial microtubule-stimulated ADP release. *Nature Cell Biology*, 2:257–260, 2000.

[43] W O Hancock and J Howard. Kinesin's processivity results from mechanical and chemical coordination between the ATP hydrolysis cycles of the two motor domains. *Proceedings of the National Academy of Science*, 96(23):13147–13152, 1999.

[44] A G Hendricks, B I Epureanu, and E Meyhöfer. Mechanistic mathematical model of kinesin under time and space fluctuating loads. *Nonlinear Dynamics*, DOI:10.1007/s11071-007-9315-1, 2007.

[45] H Hess. Towards devices powered by biomolecular motors. *Science*, 312(5775):860–861, 2006.

[46] J Howard. *Mechanics of Motor Proteins and the Cytoskeleton*. Sinauer Associates, Inc., 2001.

[47] J Howard, A J Hudspeth, and R D Vale. Movement of microtubules by single kinesin molecules. *Nature*, 342:154–158, 1989.

[48] J Howard, A J Hunt, and S Baek. Assay of microtubule movement driven by single kinesin molecules. *Methods Cell Biology*, 39:137–147, 1993.

[49] T G Huang, J Suhan, and D D Hackney. Drosophila kinesin motor domain extending to amino acid position 392 is dimeric when expressed in Escherichia coli. *Journal of Biological Chemistry*, 269:16502–16507, 1994.

[50] K H Iwasa. A two-state piezoelectric model for outer hair cell motility. *Biophysical Journal*, 81:2495–2506, 2001.

[51] A Jadbabaie, N Motee, and M Barahona. On the stability of the Kuramoto model of coupled nonlinear oscillators. *submitted to ACC*, 2004.

[52] J Jaud, F Bathe, M Schliwa, M Rief, and G Woehlke. Flexibility of the neck domain enhances kinesin-1 motility under load. *Biophysical Journal*, 91:1407–1412, 2006.

[53] F Julicher and J Prost. Spontaneous oscillations of collective molecular motors. *Physical Review Letters*, 78(23):4510–4514, 1997.

[54] R Kanada and K Sasaki. Theoretical model for motility and processivity of two-headed molecular motors. *Physical Review E*, 67:061917, 2003.

[55] H Kantz and T Schreiber. *Nonlinear Time Series Analysis*. Cambridge University Press, 1997.

[56] T M Kapoor, T U Mayer, M L Coughlin, and T J Mitchison. Probing spindle assembly mechanisms with monastrol, a small molecule inhibitor of the mitotic kinesin, Eg5. *Journal of Cell Biology*, 150(5):975–988, 2000.

[57] D Keller and C Bustamante. The mechanochemistry of molecular motors. *Biophysical Journal*, 78:541–556, 2000.

[58] J W Kerssemakers, E L Munteanu, L Laan, T L Noetzel, M E Janson, and M Dogterom. Assembly dynamics of microtubules at molecular resolution. *Nature*, 442(7103):709–712, 2005.

[59] S Klumpp, A Mielke, and C Wald. Noise-induced transport of two coupled particles. *Physical Review E*, 63:031914, 2001.

[60] H Kojima, E Muto, and T Yanagida. Mechanics of single kinesin molecules measured by optical trapping nanometry. *Biophysical Journal*, 73(4):2012–2022, 1997.

[61] A B Kolomeisky, E B Stukalin, and A A Popov. Understanding mechanochemical coupling in kinesins using first-passage time. *Physical Review E*, 71:031902, 2005.

[62] K S Kosik, L D Orecchio, B J Schnapp, H Inouye, and R L Neve. The primary structure and analysis of the squid heavy chain. *Journal of Biological Chemistry*, 265:3278–3283, 1990.

[63] S C Kou, B J Cherayil, W Min, B P English, and X S Xie. Single-molecule Michaelis-Menten equations. *Journal of Physical Chemistry B*, 109:19068–19081, 2005.

[64] F J Kull and S A Endow. Kinesin: Switch I and II and the motor mechanism. *Journal of Cell Science*, 115:15–23, 2002.

[65] F J Kull and S A Endow. A new structural state of myosin. *Trends in Biochemical Sciences*, 29(3):103–106, 2004.

[66] C Kural, H Kim, S Syed, G Goshima, V I Gelfand, and P R Selvin. Kinesin and dynein move a peroxisome in vivo: a tug-of-war or coordinated movement. *Science*, 308:1469–1472, 2005.

[67] Y Kuramoto. *Chemical Oscillations, Waves, and Turbulence*. Springer, Berlin, 1984.

[68] S A Kuznetsov, E A Vaisberg, N A Shanina, N N Magretova, V Y Chernyak, and V I Gelfand. The quaternary structure of bovine brain kinesin. *EMBO Journal*, 7:353–356, 1988.

[69] C J Lawrence, R K Dawe, K R Christie, D W Cleveland, S C Dawson, S A Endow, L S B Goldstein, H V Goodson, N Hirokawa, J Howard, R L Malmberg, J R McIntosh, H Miki, T J Mitchison, Y Okada, A S N Reddy, W M Saxton, M Schliwa, J M Scholey, R D Vale, C E Walczak, and L Wordeman. A standardized kinesin nomenclature. *Journal of Cell Biology*, 167(1):19–22, 2004.

[70] V Levi, A S Serpinskaya, E Gratton, and V I Gelfand. Organelle transport along microtubules in Xenopus Melanophores: Evidence for cooperation between multiple motors. *Biophysical Journal*, 90:318–327, January 2006.

[71] C-T Lin, M-T Kao, K Kurabayashi, and E Meyhöfer. Efficient designs for powering microscale devices with nanoscale biomolecular motors. *Small*, 2(2):281–287, 2006.

[72] T U Mayer, T M Kapoor, S J Haggarty, R W King, S L Schreiber, and T J Mitchison. Small molecule inhibitor of mitotic spindle bipolarity identified in a phenotype-based screen. *Science*, 286:971–974, 1999.

[73] E Meyhöfer and J Howard. The force generated by a single kinesin molecule against an elastic load. *The Proceedings of the National Academy of Science*, 92:574–578, 1995.

[74] W Min, B P English, G Luo, B J Cherayil, S C Kou, and X S Xie. Fluctuating enzymes: Lessons from single-molecule studies. *Accounts of Chemical Research*, 38:923–931, 2005.

[75] R E Mirollo and S H Strogatz. The spectrum of the locked state for the Kuramoto model of coupled oscillators. *Physica D*, 205:249–266, 2005.

[76] X Nan, P A Sims, P Chen, and X S Xie. Observation of individual microtubule motor steps in living cells with endocytosed quantum dots. *The Journal of Physical Chemistry B*, 109: 24220–24224, 2005.

[77] R Nitta, M Kikkawa, Y Okada, and N Hirokawa. KIF1A alternately uses two loops to bind microtubules. *Science*, 305:678–683, 2004.

[78] C S Peskin and G Oster. Coordinated hydrolysis explains the mechanical behavior of kinesin. *Biophysical Journal*, 68:202–211, 1995.

[79] A Pikovsky, M Rosenblum, and J Kurths. *Synchronization: a Universal Concept in Nonlinear Science*. Cambridge Nonlinear Sciences Series 12. Cambridge University Press, 2001.

[80] S Ray, E Meyhöfer, R A Milligan, and J Howard. Kinesin follows the microtubule's protofilament axis. *Journal of Cell Biology*, 121(5):1083–1093, 1993.

[81] S Rice, A W Lin, D Safer, C L Hart, N Naber, B O Carragher, S M Cain, E Pechatnikova, E M Wilson-Kubalek, M Whittaker, E Pae, R Cooke, E W Taylor, R A Milligan, and R D Vale. A structural change in the kinesin motor protein that drives motility. *Nature*, 402: 778–784, 1999.

[82] H Risken. *The Fokker-Planck Equation: Methods of Solution and Application*. Springer-Verlag, 2 edition, 1989.

[83] S Sack, F J Kull, and E Mandelkow. Motor proteins of the kinesin family - structures, variations, and nucleotide binding sites. *European Journal of Biochemistry*, 262(1):1–11, 1999.

[84] P B Schiff, J Fant, and S B Horwitz. Promotion of microtubule assembly in vitro by taxol. *Nature*, 277(5698):665–667, 1979.

[85] M J Schnitzer and S M Block. Kinesin hydrolyses one ATP per 8-nm step. *Letters to Nature*, 388:386–390, 1997.

[86] M J Schnitzer, K Visscher, and S M Block. Force production by single kinesin motors. *Nature Cell Biology*, 2:718–723, 2000.

[87] J M Scholey, J Heuser, J T Yang, and L S B Goldstein. Identification of globular mechanochemical heads of kinesin. *Nature*, 338:355–357, 1989.

[88] S Seiler, C Kirchner, C Horn, A Kallipolitou, G Woehlke, and M Schliwa. Cargo binding and regulatory sites in the tail of fungal conventional kinesin. *Nature Cell Biology*, 2:333–338, 2000.

[89] G B Stokin, C Lillo, T L Falzone, R G Brusch, E Rockenstein, S L Mount, R Raman, P Davies, E Masliah, D S Williams, and L S B Goldstein. Axonopathy and transport deficits early in the pathogenesis of Alzheimer's disease. *Science*, 307:1282–1288, 2005.

[90] S H Strogatz. From Kuramoto to Crawford: Exploring the onset of synchronization in populations of coupled oscillators. *Physica D*, 143:1–20, 2000.

[91] S H Strogatz. *Sync: The Emerging Science of Spontaneous Order*. Hyperion, New York, New York, 2004.

[92] S H Strogatz. *Nonlinear Dynamics and Chaos*. Perseus Publishing, 1994.

[93] S H Strogatz and I Stewart. Coupled oscillators and biological synchronization. *Scientific American*, 269(6):68–75, 1993.

[94] S H Strogatz, R E Mirollo, and P C Matthews. Coupled nonlinear oscillators below the synchronization threshold: Relaxation be generalized Landau damping. *Physical Review Letters*, 68:2730–2733, 1992.

[95] E B Stukalin and A B Kolomeisky. Dynamic transitions in coupled motor proteins. *Physical Review E*, 73:031922, 2006.

[96] E B Stukalin, H Phillips III, and A B Kolomeisky. Coupling of two motor proteins: A new motor can move faster. *Physical Review Letters*, 94:238101, 2005.

[97] K Svoboda and S M Block. Force and velocity measured for single kinesin molecules. *Cell*, 77:773–784, 1994.

[98] K Svoboda, C F Schmidt, B J Schnapp, and S M Block. Direct observation of kinesin stepping by optical trapping interferometry. *Nature*, 365:721–727, 1993.

[99] R D Vale. Myosin V motor proteins: Marching stepwise towards a mechanism. *Journal of Cell Biology*, 163(3):445–450, 2003.

[100] R D Vale. The molecular motor toolbox for intracellular transport. *Cell*, 112:467–480, 2003.

[101] R D Vale, T S Reese, and M P Sheetz. Identification of a novel force-generating protein, kinesin, involved in microtubule-based motility. *Cell*, 42:39–50, 1985.

[102] R D Vale, T Funatsu, D W Pierce, L Romberg, Y Harada, and T Yanagida. Direct observation of single kinesin molecules moving along microtubules. *Nature*, 380:451–453, 1996.

[103] M G L van den Heuvel, M P de Graaff, and C Dekker. Molecular sorting by electrical steering of mictrotubules in kinesin-coated channels. *Science*, 312:910–914, 2006.

[104] K J Verhey, D Meyer, R Deehan, J Blenis, B J Schnapp, T A Rapoport, and B Margolis. Cargo of kinesin identified as JIP scaffolding proteins and associated signaling molecules. *Journal of Cell Biology*, 152(5):959–970, 2001.

[105] K Visscher, M J Schnitzer, and S M Block. Single kinesin molecules studied with a molecular force clamp. *Nature*, 400:184–189, 1999.

[106] A Yildiz, M Tomishige, R D Vale, and P R Selvin. Kinesin walks hand-over-hand. *Science*, 303:676–678, 2004.

[107] K B Zeldovich, J F Joanny, and J Prost. Motor proteins transporting cargos. *The European Physical Journal E*, 17:155–163, 2005.

[108] J Zheng, L D Madison, D Oliver, B Fakler, and P Dallos. Prestin, the motor protein of outer hair cells. *Audiology and Neuro-ontology*, 7(1):9–12, 2002.